

## COSMIC STAR FORMATION: A SIMPLE MODEL OF THE SFRD(Z)

CESARE CHIOSI,<sup>1,2</sup> MAURO SCIARRATTA,<sup>1</sup> MAURO D'ONOFRIO,<sup>1,2</sup> EMANUELA CHIOSI,<sup>2</sup> FRANCESCA BROTTTO,<sup>1</sup>  
ROSARIA DE MICHELE,<sup>1</sup> AND VALERIA POLITINO<sup>1</sup>

<sup>1</sup>*Department of Physics and Astronomy, University of Padova, Vicolo Osservatorio 3, I-35122 Padova, Italy*

<sup>2</sup>*INAF Observatory of Padova, Vicolo Osservatorio 5, I-35122 Padova, Italy*

(Received June 7, 2017; Revised; Accepted)

Submitted to ApJ

### ABSTRACT

We investigate the evolution of the cosmic star formation rate density (SFRD) from redshift  $z=20$  to  $z=0$  and compare it with the observational one by Madau and Dickinson derived from recent compilations of UV and IR data. The theoretical SFRD( $z$ ) and its evolution are obtained using a simple model which folds together the star formation histories of prototype galaxies designed to represent real objects of different morphological type along the Hubble sequence and the hierarchical growing of structures under the action of gravity from small perturbations to large scale objects in  $\Lambda$ -CDM cosmogony, i.e. the number density of dark matter halos  $N(M, z)$ . Although the overall model is very simple and easy to set up, it provides results that well mimic those obtained from large scale N-body simulations of great complexity. The simplicity of our approach allows us to test different assumptions for the star formation law in galaxies, the effects of energy feedback from stars to interstellar gas and the efficiency of galactic winds, and also the effect of  $N(M, z)$ . The result of our analysis is that in the framework of the hierarchical assembly of galaxies the so-called time-delayed star formation under plain assumptions mainly for the energy feedback and galactic winds can reproduce the observational SFRD( $z$ ).

*Keywords:* Galaxies: evolution — Galaxies: photometry — Galaxies: star formation — Galaxies: mass function — Cosmology: large-scale structure of universe — Cosmology: dark matter

arXiv:1711.03416v1 [astro-ph.GA] 9 Nov 2017

## 1. INTRODUCTION

This paper faces the problem of the global history of star formation and chemical enrichment of the whole Universe, otherwise known as the baryon budget in galactic halos or the history of the so-called star formation rate density  $\text{SFRD}(z)$ . Since the seminal studies by [Tinsley \(1980\)](#) and [Madau et al. \(1996\)](#), the cosmic star formation has been the subject of numberless papers that are impossible to recall here. The evolution of the  $\text{SFRD}(z)$  over cosmic times is crucial to understand galaxy formation and evolution and to constrain any theory devoted to this subject ([Hopkins 2004](#); [Wilkins et al. 2008](#); [Guo et al. 2011](#); [Bouwens et al. 2012](#); [Cucciati et al. 2012](#); [Tescari et al. 2014](#); [Katsianis et al. 2017](#); [Abramson et al. 2016](#)). The evolution of the  $\text{SFRD}(z)$  is nowadays known with unprecedented accuracy up to the distant Universe thanks to the multi-wavelengths surveys carried out by many groups among which we recall [Bernardi et al. \(2010\)](#); [González et al. \(2011\)](#); [Bouwens et al. \(2012\)](#); [Lee et al. \(2011\)](#); [Smit et al. \(2012\)](#); [Santini et al. \(2012\)](#); [Schenker et al. \(2013\)](#); [van der Burg et al. \(2010\)](#); [Grupponi et al. \(2013\)](#); [Parsa et al. \(2016\)](#); [Reddy et al. \(2008\)](#); [Magnelli et al. \(2011\)](#); [Sobral et al. \(2013\)](#); [Alavi et al. \(2014\)](#); [Cucciati et al. \(2012\)](#); [Ly et al. \(2011\)](#). The situation has been recently systematically summarized and reviewed by [Madau & Dickinson \(2014\)](#) and [Katsianis et al. \(2017\)](#) to whom we refer for all details.

The interpretation of the cosmic  $\text{SFRD}(z)$  has been addressed by many theoretical studies, among which we recall [Rasera & Teyssier \(2006\)](#), [Hernquist & Springel \(2003a\)](#), and [Katsianis et al. \(2017\)](#), with either analytical or semi-analytical or hydrodynamical simulations. In particular, they investigated the effect of the energy feedback from supernovae explosions, stellar winds, and AGN activity on modeling the cosmic star formation. They made use of an improved version of the P-GADGET3 of [Springel \(2005\)](#) with chemical enrichment ([Tornatore et al. 2007](#)), supernova energy and momentum-driven galactic winds ([Puchwein & Springel 2013](#)), AGN feedback ([Springel et al. 2005a](#); [Planelles et al. 2013](#)), metal-line cooling ([Wiersma et al. 2009b,a](#)) plus molecules/metal cooling ([Maio et al. 2007](#)), supernova-driven galactic winds with feedback ([Barai et al. 2013](#)), thermal conduction ([Dolag et al. 2004](#)), and other more technical details (see [Tescari et al. 2014](#), for a more exhaustive description). In general the shape of the  $\text{SFRD}(z)$  as a function of the redshift is reproduced by the models. However, according to [Tescari et al. \(2014\)](#) the  $\text{SFRD}(z)$  is insensitive to feedback at  $z > 5$ , unlike to what happens at lower redshifts. They find that the key factor for reproducing the observational  $\text{SFRD}$  is a combination of strong supernova-driven wind and early AGN feedback in low mass galaxies. Similar conclusions

are reached by [Katsianis et al. \(2017\)](#) in the sense that the AGN feedback they adopt decreases the  $\text{SFRD}$  at  $z < 3$  but not sufficiently at higher redshift. According to them, the kind of feedback one would need to reconcile things is a strong feedback at high redshifts and a less efficient one at low redshift. They also show that variable galactic winds, which are efficient at decreasing the star formation rate (SFR) of low mass galaxies, are quite successful in reproducing the observational data.

Aims of this study. Although the theoretical  $\text{SFRD}(z)$  obtained in those studies nicely reproduces the observational one (which is not a surprise since some important physical ingredients, such as for instance the energy feedback from AGNs via the galactic winds on a galaxy’s SFR, have yielded the sought variation of the cosmic  $\text{SFRD}$  with the redshift), still we feel that the results are not yet conclusive as far as the key physical process in shaping the cosmic  $\text{SFRD}(z)$  is concerned. Casting the question in a different way, we would like to understand whether the cosmic  $\text{SFRD}(z)$  is driven more by causes of external or internal nature.

Among the external causes, chief is the gravitational building up of structures (the proto-galaxies made of dark and baryonic matter) via hierarchical aggregation which leads to a mass function of galaxies which is not the same at different redshifts. The numerical simulations of cosmic mass aggregation show that the halo mass distribution function, i.e. the relative number of galaxies per mass interval, on one hand gets steeper and steeper with mass at increasing redshift but even more important several different solution are found ([Murray et al. 2013](#), and references therein) all worth being explored.

Among the internal causes, chief are the star formation, how this varies with the total mass and the mean density of the galaxy, how the SFR varies with time within a galaxy, and the physical properties of the interstellar medium. Another important issue is whether in a galaxy the SFR always starts at maximum efficiency and declines with time so that some “quenching mechanisms” must be invoked at the very early epochs to explain the decline of the  $\text{SFRD}(z)$  at increasing redshift, or rather it starts low, grows to a maximum and then declines (typical of spheroidal systems), or alternatively it remains mild and nearly constant (such as in disk-like objects), or in some cases it goes through a series of episodes (the so-called bursting model, typical of low mass galaxies).

Finally, we would like to quantify the relative weight of the hierarchical aggregation compared to the intrinsic SFR. Most likely both concur to model the  $\text{SFRD}(z)$ , but to which extent? Investigations based on large scale numerical simulations that are possible with P-GADGET3-like codes have the gravitational aggregation built in by default so that only the effect of different prescriptions for the star formation and associated energy injection and feedback can be tested. On the other

hand, testing the effects of the various physical ingredients with direct hydrodynamical large scale simulations is expensive and time consuming. For these reasons it is still useful and interesting to address the problem in a simple fashion by means of semi-analytical model able to catch the essence of the problem.

The plan of the paper is as follows. In Section 2 we shortly review the present-day observational picture about the SFRD(z), recalling the main ways of measuring it, the various points of uncertainty, in particular the role of the stellar initial mass function (IMF), the variation of the star formation histories in galaxies of different type, and the distance determinations. In Section 3 we present the strategy of the present study aimed at deriving the SFRD(z) from three elementary building blocks: (i) the current hierarchical view of galaxy formation providing the expected number of galaxies (made of dark and baryonic matter) per unit volume (usually a  $Mpc^3$ ) presented in Section 4, (ii) simple models of galaxy formation and evolution for different values of total mass and morphological type that are presented in Section 5 (they provide the rate of star formation, mass in stars, gas content, metallicity and other useful properties of individual galaxies), and (iii) finally, the evolutionary population synthesis technique that is used to derive the magnitudes and colors of the model galaxies as function of time (redshift) that is presented in Section 6. In Section 7 we fold together the results of the previous sections, derive the cosmic SFRD and compare it to observational data. In order to highlight and single out the role played by the galaxy number density distribution and the galaxy SFR at different epochs, we perform some ad hoc simulations by varying some key assumptions and illustrate the results. Finally in Section 8 some conclusive remarks are made.

## 2. THE COSMIC STAR FORMATION RATE

The SFRD(z) we intend to investigate and reproduce is the one presented by [Madau & Dickinson \(2014\)](#), and references therein). In general, to infer the SFRD(z) from the fluxes measured in suitable pass-bands (typically UV and near and far infrared, NIR and FIR, respectively) and to express it in masses per unit time and unit volume of space, one needs some assumptions about the correlation between the measured fluxes and the SFR, the corrections for the effect of dust on absorbing part of the UV to re-emit it in the NIR and FIR, the IMF together with some hints about its constancy or variation with time and space, the kind of star formation at work on cosmic scales and Hubble time, and others details.

**Major uncertainties.** A number of problems affect the determination of the SFRD(z) among which we briefly recall:

*Stellar mass census.* Deriving the mass in stars (i.e. the underlying IMF) from their light is a cumbersome affair because it requires information on the mass to

light ratio (M/L) of the stellar populations, which in turn depends on the age, the history of star formation and the amount of dust around (extinction). In general, the conversion from light to mass is made through population synthesis models which provide the relationship between mass in stars (both luminous and faint - hence invisible), the light emitted by these, and the relative number of stars born in different generations, all contributing to the light and the mass at present day; in other words, the history of star formation. Among other things, these models depend on the IMF. On the other hand, the IMF is difficult to determine directly from the observational data for a number of reasons that do not need to be examined here (see [Madau & Dickinson 2014](#), for a detailed discussion of the issue). The obvious way out is to assume a certain IMF. The most popular one is the [Salpeter \(1955\)](#) law even though it is known to predict M/L ratios higher than observed, thus requiring deep revision of the IMF at the low mass hand (see [Kroupa et al. 1993](#); [Chabrier 2015](#); [Hennebelle & Chabrier 2011](#)). Another difficulty affecting the stellar mass census is due to the detection of low mass dusty galaxies. This means that a great portion of the stellar mass could be missing in current data.

*Variations of the star formation history in galaxies.* The star formation history (SFH) of a galaxy may change a lot over the years both on short and long timescales. As a matter of fact, young stars outshine the old ones thus affecting the total spectral energy distribution, and hence the total mass of the old stars may be largely underestimated and the effect of these can be hardly singled out.

*Distances.* Finally, the sources of observational data change with the distance so that homogeneous data sets extending from the local pool all the way up to redshift  $z \leq 10$  are not possible: For instance in the local Universe ( $0 < z < 1$ ) most of the IR data are not due to dust in star-forming regions but to dust in the ISM. This trend tends to decrease with the distance. In the redshift interval  $1 < z < 4$ , no IR data are measured for individual sources but for the hyper-luminous ones, thus heavily affecting the evaluation of the IR luminosity density. At larger redshifts essentially only data for hyper-luminous sources are available thus worsening the problem. For all these reasons, [Madau & Dickinson \(2014\)](#) limit their analysis to the redshift interval  $0 < z < 8$ .

**Analytical Fits.** In this work, we will make use of the analytical fits derived by [Madau & Dickinson \(2014\)](#) and [Madau & Fragos \(2017\)](#). Both have similar functional dependencies given by

$$SFRD(z) = \gamma_0 \frac{(1+z)^{\gamma_1}}{1 + \frac{(1+z)^{\gamma_2}}{\gamma_2}} M_{\odot} yr^{-1} Mpc^{-3} \quad (1)$$

The relation of [Madau & Dickinson \(2014\)](#) is for  $\gamma_0 = 0.015$ ,  $\gamma_1 = 2.7$ ,  $\gamma_2 = 2.9$ , and  $\gamma_3 = 5.6$  and it is shown

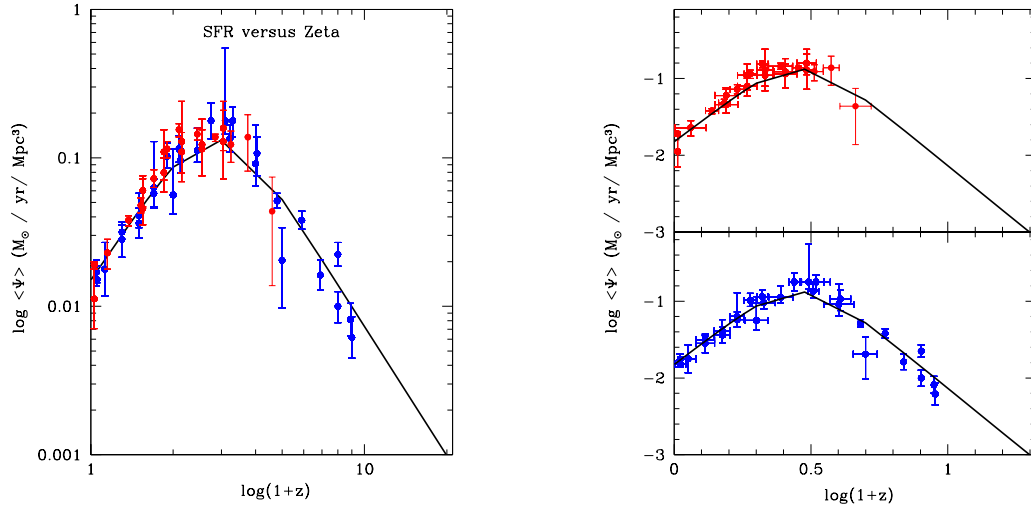


**Figure 1.** The history of cosmic star formation according to Madau & Dickinson (2014, their Fig.8). The left panel shows the rest-frame FUV+IR data (blue and red dots respectively), whereas in the right panels the same data are plotted separately. The sources of data are those listed in Table 1 of Madau & Dickinson (2014). The solid line in the three panels is the analytical best fit of the data given by Madau & Dickinson (2014).

in the three panels of Fig.1 together with the original data from the same source.

In recent times, the above relationship has been slightly revised by Madau & Fragos (2017) who used the Kroupa (2001) IMF. The new coefficients and exponents are  $\gamma_0 = 0.01$ ,  $\gamma_1 = 2.6$ ,  $\gamma_2 = 3.2$ , and  $\gamma_3 = 6.2$ . It is easy to check that the old and new relationships agree within a factor of about two. Both represent the foot-print of the past star and galaxy formation history of the Universe that needs to be deciphered (see Fig.19 for a comparison).

### 3. STRATEGY: DERIVING THE SFRD(Z) FROM FUNDAMENTAL BUILDING BLOCKS

In this study, we intend to derive the observational SFRD(z) from a small number of hypotheses or “building blocks”:

1) The cosmic scenario and the hierarchical building up of bound structures which provide the number density of DM halos of mass  $M_{DM}$  and radius  $R_{DM}$  as function of the redshift,  $N(M_{DM}, z)$ .

2) The aggregation of BM in DM halos which provides the visible component of galaxies and their star formation and chemical enrichment. This gives rise to a complicate game among several important physical processes, chief among others the gravitational contraction and collapse together with gas heating and cooling and star formation. All this requires a suitable timescale to occur so that building up of the stellar component of a galaxy cannot be instantaneous. The best simple model apt to describe this situation is the so-called “in-fall model” developed by Chiosi (1980).

3) The spectro-photometric properties of the stellar population of galaxies that will provide the evolution of spectral energy distribution as function of time, SFH and chemical enrichment. This gives us magnitudes and colors of the stellar populations in galaxies as a function of the time and/or redshift for whatsoever photometric system in use.

The SFRD(z) results from folding together the building blocks above: at each redshift we know the number density of DM halos and associated BM galaxies born in the redshift  $z_f \leq z$ , where  $z_f$  is the redshift at which the first galaxies are supposed to form ( $z = 20$  in our case). At each redshift we calculate the number density of galaxies per  $Mpc^3$  as a function of the mass of the DM halo (this soon sets the mass of the BM galaxy hosted by a DM halo). For this ideal sample of galaxies we calculate the total and mean cosmic density of star formation, metallicity, mass in stars, and luminosity emitted in any pass-band according to

$$[\mathcal{F}]_T = \int \int \mathcal{F}(M_{DM}, z, z_f) \times N(M_{DM}, z, z_f) dM_{DM} dz \quad (2)$$

$$\langle \mathcal{F} \rangle = \frac{\int \int \mathcal{F}(M_{DM}, z, z_f) \times N(M_{DM}, z, z_f) dM_{DM} dz}{\int \int N(M_{DM}, z, z_f) dM_{DM} dz} \quad (3)$$

where  $\mathcal{F}$  stands for any of the physical quantities listed above and the integrals are carried out over the range of  $M_{DM}$  and  $z_f \geq z \geq 0$  we have considered. The correspondence between the halo mass  $M_{DM}$  and the BM

galaxy mass  $M_{BM}$  inside is fixed by the cosmological model of the Universe (see below).

#### 4. FIRST BUILDING BLOCK: NUMBER OF DM HALOS AT DIFFERENT REDSHIFTS

We assume the  $\Lambda$ -CDM concordance cosmology, with values inferred from the WMAP-5 data (Hinshaw et al. 2009): flat geometry,  $H_0 = 70.5$  km/s/Mpc,  $\Omega_\Lambda = 0.72$ ,  $\Omega_m = 0.28$ ,  $\Omega_b = 0.046$  (giving a baryon ratio of  $\Omega_b/\Omega_m \simeq 0.1656$ ),  $\sigma_8 = 0.817$ , and  $n = 0.96$ . To these values for  $\Omega_m$  and  $\Omega_b$  we have the corresponding ratio between the baryonic and dark matter masses of individual galaxies  $M_{BM}/M_{DM} \simeq 0.16$  and vice versa  $M_{DM}/M_{BM} \simeq 6.12$ .

As already mentioned, the standard approach to investigate the cosmic SFRD is based on large scale cosmological N-Body simulations in the framework of a given cosmological model of the Universe ( $\Lambda$ -CDM in our case) so that the appearance, growth and subsequent aggregation of perturbations of all scales can be suitably described (Springel et al. 2005b, e.g.). The formation of DM halos and BM galaxies inside are automatically taken into account in the simulations. The price to pay is a large computational cost so that the analysis is limited to a few paradigmatic cases.

In alternative, one may adopt the strategy used by Lukić et al. (2007). Starting from the Warren et al. (2006) halo mass function (HMF), they derive the halo growth function (HGF) in the concordance  $\Lambda$ -CDM model over a wide range of redshifts (from  $z \simeq 20$  to the present) (see their Fig.2). The HGF  $N(M_{DM}, z)$  gives the number density of halos of different masses per (Mpc  $h^{-1}$ )<sup>3</sup> resulting by all creation/destruction events. By performing a large suite of nested-box N-body simulations with careful convergence and error controls, they determine the mass function and its evolution with excellent statistical and systematic errors, reaching a few percent over most of the considered redshift and mass range. The advantage of the Lukić et al. (2007) study is that it provides a halo mass distribution function,  $N(M_{DM}, z)$ , easy to use in all cases like the present one in which galaxy evolution has to be framed in a cosmological context.

In order to make use of the Lukić et al. (2007) distribution in our analysis, we fit their results with a fourth order polynomial

$$\log N(M_{DM}, z) = \sum_{j=0}^4 A_j(M_{DM}) \times z^j. \quad (4)$$

The coefficients  $A_j(M_{DM})$  are listed in Table 1. The interpolated distribution function for the number density  $N(M_{DM}, z)$  of halos per  $Mpc^3$  as a function of the mass and redshifts is shown here in Fig. 2. As expected it is identical to the original one by Lukić et al. (2007).

Although what we are going to say is well known, see the pioneer study of Press & Schechter (1974) and

Lukić et al. (2007, for ample referencing), for the sake of clarity and relevance for our discussion we note the following: (i) for each halo mass (or mass interval) the number density is small at high redshift, increases to high values towards the present, and depending on the halo mass either gets a maximum value at a certain redshift followed by a decrease (typical of low-mass halos) or it keeps increasing as in the case of high-mass halos; in other words, first creation of halos of a given mass (by spontaneous growth of perturbation to the collapse regime or by mergers) overwhelms their destruction (by mergers), whereas the opposite occurs past a certain value of the redshift, for low mass halos; (ii) at any redshift high mass halos are orders of magnitude less frequent than the low mass ones; (iii) at any redshift, the mass distribution of halos has a typical interval of existence whose upper mass end (cut-off mass) increases at decreasing redshift.

Finally it worth recalling that both the number densities  $N(M_{DM}, z)$  Lukić et al. (2007) and the SFRD( $z$ ) of Madau & Dickinson (2014) are per  $Mpc^3$  so that comparing theory with observations is less of a problem. However, owing to the many uncertainties affecting the observational data and the crudeness of the theoretical models, small adjustments of the order of a few units can be tolerated in the final comparison.

#### 5. SECOND BUILDING BLOCK: THE BM GALAXIES INSIDE DM HALOS

Given the mass distribution of DM halos as a function of the redshift and knowing the mass  $M_{BM}$  of baryons inside thanks to the cosmological proportions  $M_{BM}/M_{DM} \simeq 0.16$ , one needs a prescription to get a model galaxy out of this lump of matter. DM and BM undergo gravitational collapse, baryons cool down, accumulate towards the core, and form stars. The visible galaxy is gradually built up. The timescale needed to get to the stage of nearly complete generation of the stellar content goes from the typical free-fall time (say about 0.5 Gyr or so) to significantly longer than this (say about 2 Gyr or even longer) depending on the galaxy type (mass). The NB-TSPH simulations of Chiosi & Carraro (2002) in a monolithic-like scheme and those of Merlin & Chiosi (2006, 2007); Merlin et al. (2012) in the early hierarchical one show that at decreasing galaxy mass the SFR shifts from a single prominent early episode to ever continuous bursting-like mode as the galaxy mass and/or the over-density of the initial perturbation decreases, and that in massive and intermediate mass galaxies (with  $M_{BM}$  from  $10^{10}$  to  $10^{11} M_\odot$  or more) the building-up of the stellar component is complete up to 90% or so before  $z \simeq 2$ . These overall trends and timescales of galaxy formation have been independently found and confirmed by Thomas et al. (2005) from their analysis of the line absorptions indices in a large sample of galaxies. See also the review of Renzini (2006).

**Table 1.** Coefficients of the polynomial interpolation of the relation (4), which provides the number density of halos  $N(M_{DM}, z)$  per  $(\text{Mpc}/h)^3$ .

| Mass [ $M_\odot/h$ ] | $A_4$       | $A_3$       | $A_2$       | $A_1$       | $A_0$    |
|----------------------|-------------|-------------|-------------|-------------|----------|
| 5e7                  | -2.34275e-5 | 1.28686e-3  | -2.97961e-2 | 2.11295e-1  | 2.02908  |
| 5e8                  | -2.76999e-5 | 1.49291e-3  | -3.47013e-2 | 2.13274e-1  | 1.13553  |
| 5e9                  | -1.31118e-5 | 6.50876e-4  | -2.36972e-2 | 1.31993e-1  | 0.23807  |
| 5e10                 | -1.18729e-5 | 6.65488e-4  | -3.17079e-2 | 1.30360e-1  | -0.59744 |
| 5e11                 | -1.47246e-5 | 8.10097e-4  | -4.65279e-2 | 1.13790e-1  | -1.44571 |
| 5e12                 | 6.59657e-5  | -7.19134e-4 | -6.99445e-2 | 1.06782e-1  | -2.45684 |
| 5e13                 | -7.34568e-4 | 9.99022e-3  | -1.65888e-1 | -9.48292e-2 | -3.11701 |

**Table 2.** Expected number densities of DM halos per  $[Mpc h^{-1}]^3$  at varying the DM mass and redshift  $z$ . The DM masses are in  $M_\odot h^{-1}$ .

| $z$   | $10^7$    | $10^8$    | $10^9$    | $10^{10}$ | $10^{11}$ | $10^{12}$ | $10^{13}$ |
|-------|-----------|-----------|-----------|-----------|-----------|-----------|-----------|
| 20.00 | 0.113E+01 | 0.159E-01 | 0.482E-04 | 0.857E-08 | 0.346E-14 | 0.506E-24 | 0.000E+00 |
| 15.00 | 0.658E+01 | 0.215E+00 | 0.390E-02 | 0.111E-04 | 0.930E-09 | 0.335E-16 | 0.120E-45 |
| 10.00 | 0.240E+02 | 0.152E+01 | 0.753E-01 | 0.180E-02 | 0.762E-05 | 0.566E-09 | 0.176E-18 |
| 8.00  | 0.347E+02 | 0.274E+01 | 0.168E+00 | 0.756E-02 | 0.104E-03 | 0.103E-06 | 0.691E-13 |
| 6.00  | 0.433E+02 | 0.415E+01 | 0.293E+00 | 0.219E-01 | 0.778E-03 | 0.601E-05 | 0.568E-09 |
| 4.00  | 0.433E+02 | 0.485E+01 | 0.389E+00 | 0.419E-01 | 0.304E-02 | 0.994E-04 | 0.312E-06 |
| 2.00  | 0.319E+02 | 0.395E+01 | 0.376E+00 | 0.507E-01 | 0.585E-02 | 0.437E-03 | 0.190E-04 |
| 1.00  | 0.235E+02 | 0.299E+01 | 0.322E+00 | 0.461E-01 | 0.610E-02 | 0.554E-03 | 0.638E-04 |
| 0.80  | 0.218E+02 | 0.278E+01 | 0.309E+00 | 0.445E-01 | 0.601E-02 | 0.559E-03 | 0.755E-04 |
| 0.60  | 0.202E+02 | 0.257E+01 | 0.295E+00 | 0.427E-01 | 0.586E-02 | 0.556E-03 | 0.869E-04 |
| 0.40  | 0.185E+02 | 0.237E+01 | 0.280E+00 | 0.408E-01 | 0.568E-02 | 0.546E-03 | 0.973E-04 |
| 0.20  | 0.169E+02 | 0.217E+01 | 0.266E+00 | 0.387E-01 | 0.545E-02 | 0.529E-03 | 0.106E-03 |
| 0.00  | 0.157E+02 | 0.201E+01 | 0.254E+00 | 0.371E-01 | 0.525E-02 | 0.512E-03 | 0.111E-03 |

The infall models of galactic chemical evolution over the years have reached a very high degree of complexity and sophistication, have been applied to study galaxies of different morphological type going from early types to disks and irregulars and have proved to successfully explain many observational properties of galaxies such as chemical abundances, gas and stellar content and, with the aid of photometric synthesis tools, also magnitudes and colors. The situation has been widely reviewed by [Matteucci \(2012, 2016\)](#): we limit ourselves to mention here those developed by [Bressan et al. \(1994\)](#); [Chiosi et al. \(1998\)](#); [Tantalo et al. \(1996, 1998\)](#) for early type galaxies, and by [Portinari & Chiosi \(1999, 2000\)](#); [Fattore \(2009\)](#) for spherical and disk galaxies with radial flows of gas.

In the following, we will use models adapted to the one zone description (fully adequate to our purposes) from those elaborated by [Tantalo et al. \(1998\)](#) in spherical symmetry. Over the years many important physical phenomena have been incorporated in the chemical models, for instance gas heating by supernova explosions (both type II and type Ia), stellar winds, gas cooling by radiative emission, in order to correctly evaluate the thermal content of the gas eventually triggering the galactic winds, and finally the radial flows of gas. Only recently, the same physical processes have been included also in the N-body simulations of galaxy formation and evolution. Due to the scarce communication between the two scientific communities, the strong predicting power of

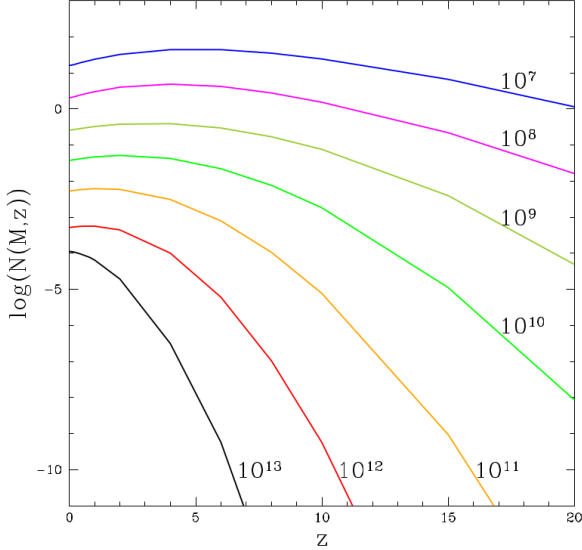


**Figure 2.** The HGF reproduced from Lukić et al. (2007). The number density of galaxies (in logarithmic scale) is in  $(\text{Mpc } h^{-1})^3$ , where  $h = H_0/100$ . Each line refers to halos with DM mass in solar units as indicated.

the costless chemical models with respect to the heavy time consuming numerical simulations has been ignored.

The essence of all infall models is the assumption of the gas accretion into the central region of the protogalaxy at a suitable rate (driven by the timescale  $\tau$ ) and of gas consumption by a Schmidt-like law of star formation. The gas accretion and consumption coupled together give rise to a time dependence of the SFR closely resembling the one resulting from the N-body simulations and the line absorption indices diagnostics. We will come back to this important issue later on in this study.

In the framework of infall models, the luminous mass  $M_{BM}$  increases with time according to

$$\frac{dM_{BM}(t)}{dt} = \dot{M}_{BM,0} \exp(-t/\tau) \quad (5)$$

where  $\tau$  is the accretion timescale. The constant  $\dot{M}_{BM,0}$  is obtained from imposing that at the galaxy age  $T_G$  the value  $M_{BM}(T_G)$  is reached:

$$\dot{M}_{BM,0} = \frac{M_{BM}(T_G)}{\tau[1 - \exp(-T_G/\tau)]} \quad (6)$$

Therefore, integrating the accretion law the time dependence of  $M_{BM}(t)$  is

$$M_{BM}(t) = \frac{M_{BM}(T_G)}{[1 - \exp(-T_G/\tau)]} [1 - \exp(-t/\tau)] \quad (7)$$

The above formalism allows us to immediately recover the *closed box* approximation letting  $\tau \rightarrow 0$ . The timescale  $\tau$  parameterizes the timescale over which the present-day mass  $M_{BM}(T_G)$  is reached. In this scheme the total mass of a galaxy at the present time is  $M_G = M_{DM} + M_{BM}(T_G)$ .

### 5.1. Basic equations of the model

We denote with  $X_i(t)$  the current mass abundance of an element  $i$  and introduce the dimensionless variables

$$G(t) = M_g(t)/M_{BM}(T_G) \quad (8)$$

and

$$G_i(t) = G(t)X_i(t), \quad (9)$$

where by definition  $\sum_i X_i(t) = 1$ .

The equations governing the time variation of the  $G_i(t)$  and hence  $X_i(t)$  are

$$\begin{aligned} \frac{dG_i(t)}{dt} = & -X_i(t)\psi(t) + \\ & \left[\frac{dG_i(t)}{dt}\right]_{star} + \left[\frac{dG_i(t)}{dt}\right]_{inf} - \left[\frac{dG_i(t)}{dt}\right]_{win} \end{aligned} \quad (10)$$

where  $\psi(t)$  is the normalized rate of star formation to be defined, and  $t$  the current galaxy age.

The four terms at the right hand side are in the order: the rate of gas consumption by star formation, the rate of gas restitution (ejecta) by stars formed in previous epochs, the rate of mass accretion by infall of primordial gas onto the system, and the finally the rate at which enriched gas leaves the system. The infall rate is given by

$$\left[\frac{dG_i(t)}{dt}\right]_{inf} = \frac{X_{inf}}{M_{BM}(T_G)} \left[\frac{dM(t)}{dt}\right]_{inf} \quad (11)$$

and it is easily derived from eqn.(5). The rate of gas ejection is formally given by

$$\left[\frac{dG_i(t)}{dt}\right]_{win} = \frac{X_i(t)}{M_{BM}(T_G)} \left[\frac{dM(t)}{dt}\right]_{win} \quad (12)$$

is usually taken to be very high (nearly instantaneous ejection of all heated up gas).

The rate of gas ejection by stars is more complicated to calculate. The correct definition of this quantity can be found in Bressan et al. (1994), Tantaló et al.

(1996), and Tantalò et al. (1998). Suffice here to mention that (i) it requires integration over the IMF to account for the different contribution from stars of different mass and lifetime  $\tau_M$ , (ii) the stellar yields are calculated according to the so-called Q-formalism (cf. Talbot & Arnett 1971, 1973); (iii) at any age  $t$ , the rate of star  $\psi(t)$  weighting the contribution from star of different mass  $M$  must be evaluated at  $t_M = t - \tau_M$ . The inclusion of Type Ia supernovae is made according to Matteucci & Greggio (1986) and it requires the specification of the mass interval and mass ratios for the binary stars progenitors of Type Ia supernovae together with the distribution function  $f(\mu)$  of their mass ratios and the percentage of such binary systems with respect to the total. The contribution from Type II supernovae is straightforward as it is incorporated in the Q-formalism. The stellar ejecta are from Marigo et al. (1996, 1998), Portinari (1998), and Portinari et al. (1998) to whom we refer for all details. The stellar lifetimes  $\tau_M$  are from the tabulations by Bertelli et al. (1994) and take the dependence of  $\tau_M$  on the initial chemical composition into account. Finally, for the purposes of this study we follow in detail only the total metallicity (the sum of the abundances by mass of all elements heavier than  $^4\text{He}$ ), shortly indicated by  $Z = \sum_{j>He} X_j$ .

Last we write the equation for the current mass of a galaxy in form of stars  $M_s(t)$ : at any age  $t$  this is given by

$$M_s(t) = M_{BM}(t) - M_g(t) \quad (13)$$

with obvious meaning of the symbols.

### 5.2. The stellar initial mass function

For this we choose the Salpeter (1955) law by number

$$\phi(M) = M^{-x} \quad (14)$$

where  $x = 2.35$ . The IMF is normalized by choosing the fraction  $\zeta$  of stars more massive than  $M_n$ , i.e. the mass interval most contributing to chemical enrichment over the whole Hubble time

$$\zeta = \frac{\int_{M_n}^{M_u} \phi(M) \times M \times dM}{\int_{M_l}^{M_u} \phi(M) \times M \times dM} \quad (15)$$

Where  $M_u$  and  $M_n$  fixed and equal to  $M_u = 100M_\odot$  and  $M_n \simeq 1M_\odot$ , the lowest mass limit  $M_l$  is left free. Following Bressan et al. (1994); Tantalò et al. (1996, 1998) good choices for  $\zeta$  are from 0.3 to 0.5 (and the values for  $M_l$  are consequently derived).

### 5.3. The star formation rate

The rate of star formation is assumed to depend on the gas mass according to

$$\Psi(t) = \frac{dM_g}{dt} = \nu M_g(t)^k \quad (16)$$

where  $\nu$  and  $k$  are adjustable parameters.

The SFR normalized to  $M_{BM}(T_G)$  becomes

$$\psi(t) = \nu M_{BM}(T_G)^{k-1} G(t)^k \quad (17)$$

Linear and quadratic dependencies of the SFR on the gas content,  $k = 1$  and  $k = 2$  respectively, were first proposed by Schmidt (1959) and have been adopted ever since because of their simplicity (see Larson 1991, for a classical review of the subject). We adopt here  $k = 1$ .

With the law of star formation of equation (16), the resulting time dependence of  $\psi(t)$  is driven by the rate of mass accretion onto the system. In the closed-box description, the SFR is maximum at the beginning, and since then it continuously decreases until galactic winds occur. In the infall model, owing to the competition between the rate of gas infall and gas consumption by star formation, the rate of star formation starts small, increases to a maximum and then declines. The age at which the peak occurs, shortly indicated by  $T_P$ , approximately corresponds to the infall timescale  $\tau$ .

Finally,  $\nu$  is the efficiency parameter of the star forming process. Its physical meaning is better understood by casting the SFR in a slightly different fashion. One can identify  $dt$  with the timescale  $\tau$  of the mass accretion rate and assume  $k = 1$

$$\begin{aligned} \Psi(t) = \frac{dM_g}{dt} = \nu M_g(t)^k &\Rightarrow \frac{\Delta M_g}{M_g} = \tau \nu \\ &\Rightarrow \simeq \frac{\Delta M_s}{M_g} = \tau \nu \end{aligned} \quad (18)$$

where the ratio  $\Delta M_s/M_g$  is the mass of gas already converted to stars with respect to the mass of the left-over gas. Furthermore, if the accretion  $\tau$  is identified with the infall timescale  $t_{ff}$  of a galaxy we may get rough estimates of the specific star formation efficiency. The infall timescale of a galaxy can be approximated to the collapse timescale of primordial perturbations which depends on the redshift but is independent on the galaxy mass. Rough estimates of  $\tau$  yield values ranging from 0.05 to 0.1 Gyr when the galaxy formation redshift is in the interval 20 to 1. This in turn implies  $\nu \simeq 20$  to 1 to assemble a typical  $10^{12} M_\odot$  galaxy. This efficiency is lowered by a factor of ten at least if the mass assembly is diluted over the Hubble time.

According to Cassarà et al. (2016) the shape of SFR as a function of time can be schematically grouped according to the value taken by the ratio of the two parameters  $\tau$  and  $\nu$  (see Fig.2 of Cassarà et al. 2016). With the above laws of gas accretion and star formation, they are able to model two main types of objects: (i) in bulge-like models, characterized by high values of  $\nu$  and low values of  $\tau$  (ratios  $\tau/\nu \leq 0.1$ ), the SFR increases to a peak on a relatively short timescale (on average 0.5 Gyr), and soon after declines. These models reproduce the chemical pattern in the gas of early-type galaxies at



both low (Piovan et al. 2006a,b,c; Pipino & Matteucci 2011) and high redshift (e.g. Matteucci & Pipino 2002; Pipino & Matteucci 2011); (ii) in the disk-like models, characterized by low values of  $\nu$  together with high values of  $\tau$  (ratios  $\tau/\nu \geq 1$ ), the SFR shows a slow rise followed by a slow decline. These models could well mimic disk and to some extent also irregular galaxies in the local Universe (Piovan et al. 2006a,b,c; Pipino et al. 2013).

Finally, we like to mention that a functional form for the SFR that could mimic the above systematic variation with galaxy type (mass) is the so-called delayed exponentially declining law

$$\Psi(t) \propto \frac{t}{\tau} \exp(-\frac{t}{\tau}). \quad (19)$$

In this framework, the Schmidt law is the link between the gas accretion by infall and the gas consumption by star formation. By varying the parameters  $\tau$  and  $\nu$  we may model different types of galaxies (Buzzoni 2002).

Basing on these considerations and taking the results of NB-TSPH simulations by Chiosi & Carraro (2002), Merlin & Chiosi (2006, 2007), and Merlin et al. (2012) as reference templates for the SFH in galaxies of different mass and morphological types, we calculate chemical models for different combinations of  $\tau$  and  $\nu$  that are meant to cover the whole Hubble sequence of galaxies.

#### 5.4. Onset of galactic winds: energy feedback and gas heating-cooling

Long ago Larson (1974) postulated that the present-day Color-Magnitude Relations of elliptical galaxies (see Bower et al. 1992; Kodama et al. 1999, 2001; Terlevich et al. 2001, and references) could be the result of galactic winds powered by supernova explosions thus initiating a long series of chemo-spectrophotometric models of elliptical galaxies standing on this idea (Saito 1979a,b; Matteucci & Tornambé 1987; Arimoto & Yoshii 1987; Angeletti & Giannone 1990; Mihara & Takahara 1994; Matteucci 1994; Gibson 1998; Gibson & Matteucci 1997, and references therein). In brief, gas is let escape from the galaxy and star formation is supposed to halt when the total thermal energy of the gas equates its gravitational binding energy. The same scheme is adopted here in the models that take galactic winds into account, i.e. the term  $[\frac{dG_i(t)}{dt}]_{win}$  in eqn. (10) is at work.

The thermal energy of the gas is mainly due to three contributions, namely Type Ia and II supernovae and stellar winds from massive stars:

$$E_{th}(t) = \sum_J E_{th}(t)_J \quad (20)$$

where  $J \equiv \text{SNI}$  for type Ia supernovae,  $J \equiv \text{SNII}$  for type II supernovae, and  $J \equiv W$  for stellar winds; each term has a similar dependence

$$E_{th}(t)_J = \int_0^t \epsilon_J(t-t') R_J(t') M_{BM}(T_G) dt' \quad (21)$$

with obvious meaning of the symbols. The quantities  $\epsilon_J(t-t')$ 's and  $R_J(t)$ 's are the energies emitted by a supernova and/or stellar wind event and the corresponding production rates, respectively. As the production rates are functions of the dimensionless variables  $G_i(t)$ , the normalization factor  $M_{BM}$  is required to calculate the energy in physical units. The production rates can be easily derived from the equations governing the chemical evolution. The emitted energies incorporate the cooling laws of supernova remnants and stellar winds by radiative cooling processes according to expression used by Tantaló et al. (1998).

Finally, star formation and chemical enrichment of the model galaxies are halted, and the remaining gas is supposed to be expelled (winds) when the condition

$$E_{th}(t) \geq |\Omega_g(t)| \quad (22)$$

is verified.

#### 5.5. Gravitational potential of DM and BM

To calculate the gravitational energy of the gas we make use of the analytical dynamical models of Bertin et al. (1992) and Saglia et al. (1992) and adapt them to our case. DM is supposed to be already in situ, whereas the BM is supposed to fall into the gravitational well of the former and soon to reach the equilibrium configuration so that at each instant the description of Bertin et al. (1992) and Saglia et al. (1992) can be applied. In this description of galactic structure, the mass and radius of the DM,  $M_{DM}$  and  $R_{DM}$  respectively, are related to those of the BM,  $M_{BM}$  and  $R_{BM}$ , by the relation

$$\frac{M_{BM}(t)}{M_{DM}} \geq \frac{1}{2\pi} \left( \frac{R_{BM}(t)}{R_{DM}} \right) \left[ 1 + 1.37 \left( \frac{R_{BM}(t)}{R_{DM}} \right) \right] \quad (23)$$

and the binding gravitational energy of the gas is given by

$$\Omega_g(t) = -\alpha_{BM} G \frac{M_g(t) M_{BM}(t)}{R_{BM}(t)} - G \frac{M_g(t) M_{DM}}{R_{BM}(t)} \Omega'_{BDM} \quad (24)$$

where  $G$  is the gravitational constant,  $M_g(t)$  the current value of the gas mass,  $\alpha_{BM}$  a numerical factor  $\simeq 0.5$ , and

$$\Omega'_{BDM} = \frac{1}{2\pi} \left( \frac{R_{BM}(t)}{R_{DM}} \right) \left[ 1 + 1.37 \left( \frac{R_{BM}(t)}{R_{DM}} \right) \right] \quad (25)$$

the contribution to the gravitational energy given by the presence of DM. According to Bertin et al. (1992) and Saglia et al. (1992), in equilibrium conditions  $M_{BM}/M_{DM} \simeq R_{BM}/R_{DM}$ . With the current estimates of  $M_{DM}$  and  $M_{BM}$  of the  $\Lambda$ -CDM cosmogony both ratios are equal to 0.16. With these values, the factor  $\Omega'_{BDM} = 0.04$  so that the total correction to the gravitational energy of the gas (eq. 24) does not exceed 0.3 of the term for the luminous mass.

### 5.6. General remarks on the galactic models

**Mass homology.** It is worth noting that with the above formalism, in absence of galactic winds all the models are *homologous in mass* in the sense that the same solution (current fractional gas and star mass) applies to galaxies of different mass provided suitably rescaled to the total asymptotic baryonic mass, i.e. the total baryonic mass reached at  $t = T_G$ . The same technique can also be used in presence of galactic winds by suitably rescaling the asymptotic mass to the real value i.e. subtracted by the amount of gas mass definitely lost by the system in form of galactic winds.

**Specific star formation rate.** It is also worth noticing that with above assumptions the SFR in use is the specific star formation rate (SFR per unit baryonic mass, SSFR) which depends on three parameters, i.e.  $\nu$ ,  $\tau$  and  $T_P$ . Since  $\tau$  and  $T_P$  are correlated, each galaxy model here is characterized here only by the parameters  $\nu$  and  $\tau$ .

**Groups of galaxy models.** For the purposes of this study we have calculated three groups of models, labeled A, B and C:

*Group A.* In the models of group A, we assume that all galaxies begin their evolutionary history at redshift  $z=20$  and suppose that the mass accretion timescale  $\tau$  corresponds to the free-fall timescale for the  $\rho_{200}$  overdensity of the proto-galaxy with respect to the surrounding medium at this value of the redshift. The free-fall timescale is given by

$$t_{ff}(z) = \sqrt{\frac{3\pi}{32G\rho_{200}}} \quad (26)$$

for the homologous collapse of a homogeneous sphere of gas. This timescale is the same for all galaxies independently of their mass. The free-fall timescale  $t_{ff}(z)$  goes from about  $3.5 \times 10^7$  yrs at  $z=20$  to about  $1.0 \times 10^9$  yrs at  $z = 1$ .

For the star formation efficiency parameter  $\nu$  we adopt the constant value  $\nu = 10$ . Owing to the very short mass accretion timescale and high value of  $\nu$  these models are very similar to the ideal situation of the closed-box approximation. The baryonic mass of the models spans the range  $10^7$  to  $10^{12} M_\odot$ .

*Group B.* At the light of the considerations on the type of SFH in real galaxies, in models of group B we adopt values for the accretion timescale  $\tau$  ranging from

6 Gyr to 2 Gyr as the baryonic mass increases from  $10^7 M_\odot$  to  $10^{12} M_\odot$ , but keep unchanged the value for the parameter  $\nu$ , i.e.  $\nu = 10$  for all the models. Since the ratio  $\tau/\nu$  of the models of groups A and B is always lower than one, they are best suited to represent early type objects of any mass going from dwarfs to bulges and massive ellipticals (Cassarà et al. 2016).

*Group C.* Finally, the models of Group C more closely follow the classification by Cassarà et al. (2016) who rank the galaxy SFR by means of the ratio  $\tau/\nu$ . First of all, we stretch the interval of the accretion timescale  $\tau$  assigned to each BM mass. It goes now from 2 Gyr for the  $M_{BM} = 10^{12} M_\odot$  galaxy to 10 Gyr for the  $M_{BM} = 10^7 M_\odot$ . Second, for each value of  $\tau$  we explore three values of  $\nu$ , namely  $\nu = 0.1, 1, \text{ and } 10$ . In this way we can model galaxies along the whole Hubble sequence by varying the ratio  $\tau/\nu$  depending on the galaxy mass: low values for the most massive ones corresponding to the massive early types, intermediate values for the less massive ones (going from intermediate early type to massive spirals), and high values for the less massive galaxies like low spirals and irregulars. Group C partially overlaps group B.

It goes without saying that other combinations of two out of the three parameters ( $\tau$ ,  $\nu$ , and hence  $\tau/\nu$ ) are possible. Since the aim here is to calculate galaxy models whose SFR and SFH closely resemble the ones observed in real galaxies, the choice we have made is fully adequate to our purposes.

Finally, we like to point out that the models of Group A are meant to represent a sort of reference sample corresponding to the ideal situation of the closed-box approximation. They will be used only to evaluate the effects on the SFRD( $z$ ) of an exponentially decreasing rate of star formation.

Table 3 lists all the parameters adopted for the chemical models in usage.

### 5.7. Results for the chemical models

The model galaxies are calculated from  $z_f = 20$  to  $z = 0$  i.e. from the rest-frame age  $t = 0$  Gyr to the maximum age of  $T_G = 13.75$  Gyr where  $T_G = t_u(z = 0) - t_u(z = z_f)$  with  $t_u(z)$  being the age of the Universe for the adopted cosmological model.

If for any reason, we need to change the redshift of galaxy formation from  $z_f$  to  $z_f^* \leq z_f$  (keeping unchanged all other input parameters) the same models can be used provided their rest-frame age is simply limited to the interval from  $t = 0$  at  $z_f^*$  to  $T_G^* = T_{G,(z_f=20)} - t_u(z_f^*)$ , where  $t_u(z_f^*)$  is the age of the universe at  $z = z_f^*$ . In other words, at  $z = 0$  the new galaxy is younger than the previous one.

On purpose, in this first step of the analysis, the occurrence of galactic winds is not considered. This means that the energy input from Type II and Type Ia supernovae and galactic winds are turned off so that star formation can occur all over the life of galaxies.

**Table 3.** Parameters adopted in the chemical models. Masses are in  $M_\odot$ , the timescale  $\tau$  is in Gyr, and the radii  $R_{BM}$  and  $R_{DM}$  are in kpc.

| $M_{BM}$  | $M_{DM}$           | $R_{BM}$ | $R_{DM}$ | $\zeta$ | $\tau$ | $\nu$ | $\tau/\nu$ | $\tau$  | $\nu$ | $\tau/\nu$ | $\tau$  | $\nu$ | $\tau/\nu$ |
|-----------|--------------------|----------|----------|---------|--------|-------|------------|---------|-------|------------|---------|-------|------------|
|           |                    |          |          |         |        |       | Group A    | Group B |       |            | Group C |       |            |
| $10^7$    | $6 \times 10^7$    | 0.13     | 1.35     | 0.3     | 0.01   | 10.0  | 0.003      | 6.0     | 10.0  | 0.6        | 10.0    | 0.1   | 100        |
|           |                    |          |          |         |        |       |            |         |       |            | 10.0    | 1.0   | 10         |
|           |                    |          |          |         |        |       |            |         |       |            | 10.0    | 10.0  | 1          |
| $10^8$    | $6 \times 10^8$    | 0.28     | 2.90     | 0.3     | 0.01   | 10.0  | 0.003      | 5.0     | 10.0  | 0.5        | 8.0     | 0.1   | 80         |
|           |                    |          |          |         |        |       |            |         |       |            | 8.0     | 1.0   | 8          |
|           |                    |          |          |         |        |       |            |         |       |            | 8.0     | 10.0  | 0.8        |
| $10^9$    | $6 \times 10^9$    | 0.61     | 6.26     | 0.3     | 0.01   | 10.0  | 0.003      | 4.0     | 10.0  | 0.4        | 6.0     | 0.1   | 60         |
|           |                    |          |          |         |        |       |            |         |       |            | 6.0     | 1.0   | 6          |
|           |                    |          |          |         |        |       |            |         |       |            | 6.0     | 10.0  | 0.6        |
| $10^{10}$ | $6 \times 10^{10}$ | 1.32     | 13.48    | 0.3     | 0.01   | 10.0  | 0.003      | 3.0     | 10.0  | 0.3        | 4.0     | 0.1   | 40         |
|           |                    |          |          |         |        |       |            |         |       |            | 4.0     | 1.0   | 4          |
|           |                    |          |          |         |        |       |            |         |       |            | 4.0     | 10.0  | 0.4        |
| $10^{11}$ | $6 \times 10^{11}$ | 2.85     | 29.04    | 0.3     | 0.01   | 10.0  | 0.003      | 2.5     | 10.0  | 0.2        | 3.0     | 0.1   | 30         |
|           |                    |          |          |         |        |       |            |         |       |            | 3.0     | 1.0   | 3          |
|           |                    |          |          |         |        |       |            |         |       |            | 3.0     | 10.0  | 0.3        |
| $10^{12}$ | $6 \times 10^{12}$ | 6.13     | 62.53    | 0.3     | 0.01   | 10.0  | 0.003      | 2.0     | 10.0  | 0.2        | 2.0     | 0.1   | 20         |
|           |                    |          |          |         |        |       |            |         |       |            | 2.0     | 1.0   | 2          |
|           |                    |          |          |         |        |       |            |         |       |            | 2.0     | 10.0  | 0.2        |

Finally, the discussion below is limited to the models of case B. Those of cases A and C have similar trends and behaviour.

**Star formation.** The specific (in units of  $yr^{-1}$ ) and true star formation (in  $M_\odot yr^{-1}$ ) of the model galaxies are shown in the left and right panels of Fig. 3. As expected, the SSFRs look very similar to each other, whereas the true rates may significantly change with the galaxy mass. From now on, different values of  $M_G$  are identified in all figures with the following colors: blue ( $10^7 M_\odot$ ), magenta ( $10^8 M_\odot$ ), olive green ( $10^9 M_\odot$ ), green ( $10^{10} M_\odot$ ), orange ( $10^{11} M_\odot$ ) and red ( $10^{12} M_\odot$ ).

**Metallicity.** The temporal variation of the metallicity  $Z$  for the model galaxies is shown in Fig. 4. Owing to the rather high value of  $\nu$  and parameter  $\zeta$  of the IMF normalization, high metallicities are built up in the galaxies. This is less of a problem because by lowering  $\nu$  and/or  $\zeta$  one would obtain similar results but lower values of the metallicity at the present time without changing the overall behavior of the solution.

**Gas and Star contents.** Finally, in Fig. 5 we show the temporal variation of the fractional masses of gas (bottom panel) and stars (top panel) for the models of

group B. The timescale of mass accretion varies with the galaxy mass as reported in Table 3. The intrinsic efficiency of star formation is the same for the models on display (i.e.  $\nu=10$ ). Because of the high efficiency of star formation, all the models have the peak of activity within the first Gyr of their lifetime.

**The role of  $\nu$ .** Concluding this section, it is worth commenting on the role of the intrinsic efficiency  $\nu$  in shaping the final time-dependence of the SFR in infall models of galaxy formation and evolution. So far the discussion of the results for groups B and C has been limited to models with efficient SFR represented here by all the cases with  $\nu = 10$ . The peak of activity is always confined within the first Gyr. Clearly for  $\nu = 10$  case C does not differ too much from case B. We give the preference to this particular choice for the parameter  $\nu$  in view of the discussion below concerning the SFRD(z).

In any case it is worth emphasizing that the role of  $\nu$  is of paramount importance in shaping the overall time-dependence of the SFR. The situation is best illustrated in Fig. 6 that displays the SFR vs time of the  $1 \times 10^{12} M_\odot$  and  $1 \times 10^8 M_\odot$  galaxies of Group C (three values of  $\nu$  for each case). The models gradually change

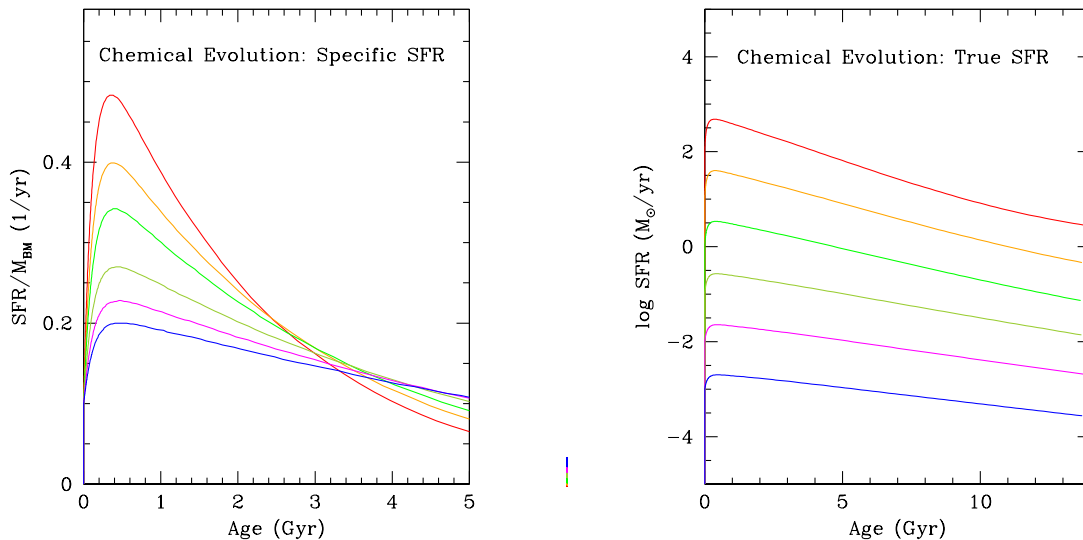


**Figure 3.** Left Panel: The SSFR of models B in  $yr^{-1}$  for the galaxies of different  $M_{BM}$ , different accretion (collapse) timescale  $\tau$  and efficiency  $\nu = 10$ . The mass  $M_{BM}$  increases from  $10^7$  to  $10^{12} M_{\odot}$  from the bottom to the top. No galactic winds are supposed to occur. The time is the age<sub>B</sub> of the galaxy in the rest-frame. Right Panel: The same as in the left panel but for the true SFR in units of  $M_{\odot} yr^{-1}$ .

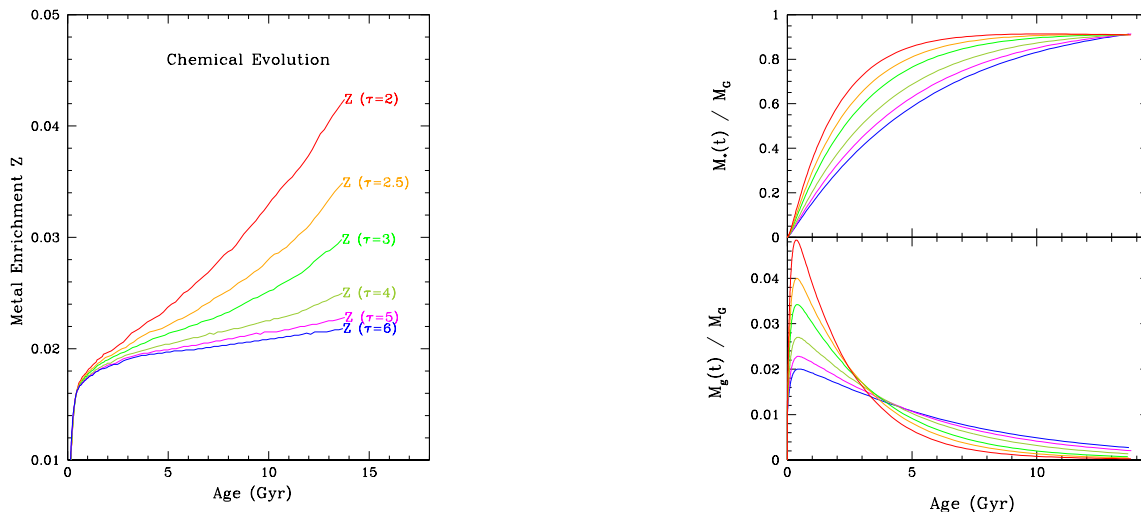


**Figure 4.** The metallicity vs time relation for the galaxies of group B with different  $M_{BM}$ , different accretion timescale  $\tau$  and efficiency  $\nu = 10$ . No galactic winds are supposed to occur. The mass  $M_{BM}$  increases from  $10^7$  to  $10^{12} M_{\odot}$  from the bottom to the top.

**Figure 5.** The gas and star content vs time relationships for the galaxies belonging to group B with different  $M_{BM}$ , different accretion timescale  $\tau$  and efficiency  $\nu = 10$ . The mass  $M_{BM}$  increases from  $10^7$  to  $10^{12} M_{\odot}$  from the bottom to the top.

their SFR from early peaked to ever-continuing according to the value of the ratio  $\tau/\nu$ , in other words along the Hubble sequence of galaxies passing from early types (low ratios  $\tau/\nu$ ) to disk-like objects (intermediate ratios  $\tau/\nu$ ), and finally to irregulars (high ratios  $\tau/\nu$ ). This trend of the star formation was suggested by Sandage

(1986), examining the SFR in galaxies of different types, and more recently confirmed by studies of SFHs based on absorption line indices by Thomas et al. (2005), and NB-TSPH numerical models of galaxy formation and evolution (Chiosi & Carraro 2002; Merlin et al. 2012).

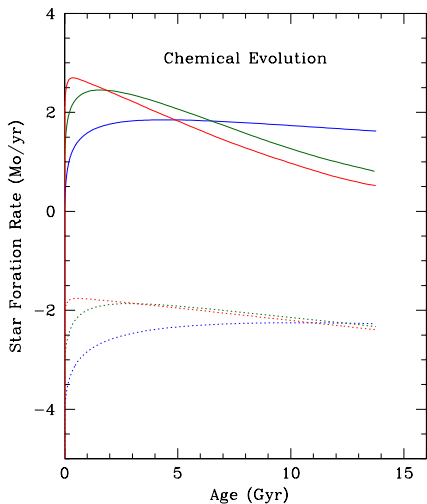


**Figure 6.** The SFR versus time relationship for the galaxies of different  $M_{BM}$  belonging to group C at varying  $\tau$  and  $\nu$ . Two values of the galaxy mass (baryonic component) are considered, namely  $10^8 M_\odot$  and  $10^{12} M_\odot$ . The values of  $\tau$  and  $\nu$  are listed in Table 3.

### 5.8. Remarks on the star formation rate

As already mentioned, the time dependence of our SFR is the delayed exponential law, see eq. (19), which is implicit to the galactic chemical models with gas accretion. The reasons why the simple exponential law,

$$\Psi(t) \propto \frac{1}{\tau} \exp\left(-\frac{t}{\tau}\right), \quad (27)$$

adopted long ago by Tinsley (1972) and in usage even today, must be abandoned have been discussed many times (see the classical studies by Lynden-Bell (1975), Chiosi (1980) and the recent review by Matteucci (2016) so that they are not repeated here).

In favor of the time delayed exponential law were the original models by Chiosi (1980) and the long list of studies dedicated to the evolution of chemical elements in galaxies of different morphological type, going from bulges and early-type objects to disk and even irregular galaxies (see Matteucci 2012, 2016, for exhaustive reviews and referencing of this issue). In support to the delayed exponential law is also the study of Gavazzi et al. (2002) with the spectro-photometric data of galaxies in the Virgo cluster.

These classical analytical representations of the SFR have been recently questioned by Oemler et al. (2013) basing their analyses on the SSFR in the redshift interval  $z \leq 1$ . They concluded that the standard laws cannot explain both the tail of high specific SFR at  $z=1$  and the low value we see today at  $z=0$ . They also argued that the starburst hypothesis cannot solve the problem. Gladders et al. (2013) argue that a log-normal SFH of

galaxies successfully describes both the SFRD over cosmic times and the present-day distribution of the SSFR of galaxies and the evolution of this quantity up to  $z \simeq 1$ . The log-normal SFR law they assume is

$$SFRD(t) \propto \frac{1}{t\tau} \exp\left[-\frac{(\ln(t) - T_0)^2}{2\tau}\right] \quad (28)$$

where  $T_0$  and  $\tau$  (not to be mistaken with the timescale of gas accretion in galaxies) are the cosmic SFRD's half mass time and width [in units of  $\ln(\text{time})$ ]. Basing on the notion that log-normal laws seem to be ubiquitous in Nature (Limpert et al. 2001), they take the SDSS sample of local galaxies (2094 objects), assign them a log-normal SFR, and derive for each object the SFR (i.e. the parameters  $T_0$  and  $\tau$ ), while ensuring that the ensemble of SFRs summed to the SFRD. Abramson et al. (2016) go ahead along this line of reasoning. Adding and folding together a large number of log-normal SFHs parameterized by  $T_0$  and  $\tau$ , they argue that this simple minded model reproduces (i) the stellar mass functions at  $z \leq 8$ ; (ii) the slope of the SFR vs stellar mass relation (the Galaxy Main Sequence) at  $z \leq 6$ ; (iii) galaxy downsizing; (iv) and a correlation between the formation timescale and the SSFR( $M_s, t$ ).

In our view, the straight inference of a log-normal SFR in single galaxies contributing to the total cosmic SFRD is somewhat arbitrary and misleading. The cosmic SFRD is not the simple summation of that of many galaxy SFRs because each galaxy may differ from the others nor all types of galaxy occur in equal number, but it results from the number weighted summation of many objects of different type and SFHs (see below). The SFR of a galaxy might not be lognormal and yet the cumulative effect of many of them may turn out to look as a log-normal distribution. For these reasons we prefer to describe the SFR of galaxies as independent entities with the time-delayed law.

## 6. THIRD BUILDING BLOCK: PHOTOMETRY

The integrated monochromatic flux generated by the stellar content of a galaxy of age  $T$  is defined as

$$F_\lambda(T) = \int_0^T \Psi[t, Z(t)] sp_\lambda[\tau', Z(\tau')] dt \quad (29)$$

where  $\Psi[t, Z(t)]$  is the SFR at the current age  $t$  and metal content  $Z$  (chemical composition in general),  $sp_\lambda[\tau', Z(\tau')]$  the integrated monochromatic flux of single stellar population (i.e. of a coeval, chemically homogeneous assembly of stars, shortly named SSP) with age  $\tau'$  and metallicity  $Z(\tau')$ , and finally  $\tau' = T - t$ . The flux of a SSP is in turn given

$$sp_\lambda[\tau', Z(\tau')] = \int_{M_l}^{M_u} \phi(M) f_\lambda[M, \tau', Z(\tau')] dM \quad (30)$$

where  $\phi(M)$  is the stellar IMF and  $f_\lambda(M, \tau', Z)$  the monochromatic flux of a star of mass  $M$ , metallicity

$Z$ , and age  $\tau' = T - t$ .  $M_l$  and  $M_u$  respectively, define the mass range within which stars are generated by each event of star formation. The metallicity dependence of the rate of star formation  $\Psi(t, Z)$  is customarily neglected and equally for the time and metallicity dependencies of the IMF.

The flux of a SSP,  $sp_\lambda(\tau', Z)$ , is calculated by integrating equation (30) along an isochrone of age  $\tau'$  populated by “virtual stars” with luminosity  $L$ , effective temperature  $T_{eff}$ , mass  $M$ , age  $\tau'$ , and composition  $Z$ . For any star along an isochrone, the relations connecting luminosity, effective temperature, and age are derived from the library of stellar models, while the flux  $f_\lambda(M, \tau', Z)$  emitted by such a star is obtained from the library of stellar spectra. Sources of stellar tracks, isochrones, spectra, and SSPs in different photometric systems are from Bertelli et al. (2008, 2009).

**Cosmological evolution of magnitudes and colours.** In the course of this study, we need the magnitudes and colors of the galaxies not only in the rest-frame but also as function of the redshift. Following Guiderdoni & Rocca-Volmerange (1987), the apparent magnitude of a galaxy at redshift  $z$  in a pass-band  $\Delta\lambda$  is

$$m(z) = (m - M)_{bol}(z) + K(z) + E(z) + M(0, t_0) \quad (31)$$

where  $K(z)$  and  $E(z)$  are the cosmological and evolutionary corrections

$$K(z) = M(z, t_0) - M(0, t_0) \quad (32)$$

$$E(z) = M(z, t_z) - M(z, t_0) \quad (33)$$

and where  $M(0, t_0)$  is the absolute magnitude in the pass-band  $\Delta\lambda$  derived from the rest-frame spectrum of the galaxy at the current time,  $M(z, t_0)$  is the absolute magnitude in the pass-band  $\Delta\lambda$  derived from the spectrum of the galaxy at the current time but redshifted at  $z$ , and  $M(z, t_z)$  is the absolute magnitude in the pass-band  $\Delta\lambda$  obtained from the spectrum of the galaxy at the time  $t_z$  and redshifted at  $z$ .

## 7. THE COSMIC STAR FORMATION RATE FROM THEORY

It is worth emphasizing from the very beginning that in the course of the analysis and companion discussion we will use two mass scales: (i) The scale of the halo masses, i.e. we will refer to galaxies by their halo mass which is roughly coincident with the total mass ( $M_G \equiv M_{DM} + M_{BM} \simeq M_{DM}$ ) to determine the number of halos per unit volume as a function of the halo mass and redshift. (ii) The scale of the baryonic component hosted by a halo, made of gas and stars. This scale will be used to read from the sample of chemical models their SFR and photometric properties (magnitudes and

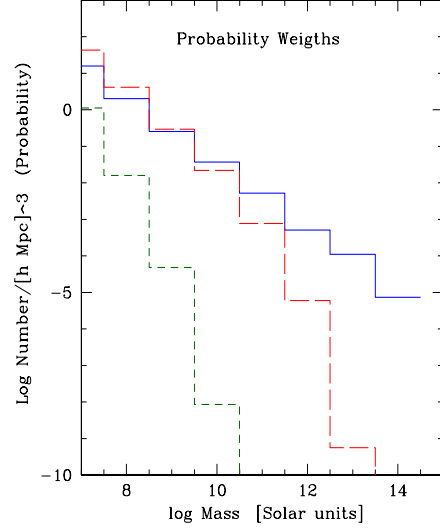


**Figure 7.** The expected number of DM halos as a function of the halo mass  $M_{DM}$  at three selected values of the redshift, namely  $z=20$  (short dashed line in dark green),  $z=6$  (long dashed line in red), and  $z=0$  (solid blue line).

colors) as a function of the BM mass, age, redshift, etc. The relationship between the two mass scales is given in the first two columns of Table 3.

Second, we will use the grids of models of the group B, choosing the one appropriate to the mass halo, according to the mass scale  $M_{BM} \simeq M_{DM}/6$ . We have already described these models in the previous section. However, we recall here that for each model we know both the SFR and the SSFR, the abundance of metals  $Z(t)$  (for the present aims the total metallicity is fully adequate), the mass in gas  $M_g(t)$  and the mass in stars  $M_s(t)$ , the integrated magnitudes in the pass-bands  $M_{\Delta\lambda}$  of the Johnson-Cousins and/or HST-WFPC photometric systems, the cosmological evolution of these magnitudes, i.e. the  $K_{\Delta\lambda}$  and  $E_{\Delta\lambda}$  corrections as a function of the redshift.

It is worth recalling here that these models not only fit the main average properties of the galaxies in the local and distant Universe, see for instance Bressan et al. (1994), Tantaló et al. (1998), and Tantaló et al. (2010), but also their SFHs agree with the results from NB-TSPH simulations of galaxy formation in cosmological context and according to the so-called early hierarchical scheme (Chiosi & Carraro 2002; Merlin & Chiosi 2006, 2007; Merlin et al. 2012). Therefore, the simple infall models presented here can be safely used to study the mean properties of galaxies in the context of the early hierarchical view of galaxy formation and evolution.

### 7.1. Distribution of halos in number and mass

We start the analysis by looking at the mass distribution of the DM halos at each value of the redshift. This is simply derived as the number of DM halos within a small interval  $\Delta z$  centered at few selected values of the redshift ( $\Delta z = 0.02$ ). The results are listed in Table 2 and are plotted in Fig. 7. The visual inspection of Fig. 2 yields a qualitative estimate of the maximum value of the mass distribution at each redshift, which means that DM halos with mass in excess of this value have such a low probability of occurrence that they can be neglected for any practical purpose. The histograms of Fig. 7 shows the comoving number density of halos as a function of the halo mass for three selected values of the redshift, namely  $z=20$  (short dashed line),  $z=6$  (long dashed line) and  $z=0$  (solid line). The mass distribution for all other values of redshift can be easily derived from the entries of Table 2. It is worth calling the attention on the steeper decrease of the number of halos at increasing halo mass and increasing redshift. While for  $z=0$  each step of the histogram roughly decreases by the same amount, this is not the case for  $z=6$  and higher in which the steps decrease more and more at increasing halo mass. This behavior of the number frequency distribution will have far reaching consequences.

### 7.2. The reference case for the SFRD(z)

In Fig. 8 we present three groups of data:

(i) The integrated absolute U magnitude of the model galaxies as a function of redshift (on logarithmic scale); each galaxy is indicated with a different color code. As expected the absolute magnitude first decreases (the luminosity increases) and then increases (the luminosity decreases) as the redshift decreases toward zero. The peak in the luminosity occurs when the rate of star formation is maximum.

(ii) The total luminosity and total magnitude in the U-pass-bands of all the galaxies present in the ideal sample contained in  $1 \text{ Mpc}^3$  according to the Lukić et al. (2007) statistics. The total U flux is given by

$$[F_{\Delta\lambda}(z_j)]_T = \sum_i N_i(M_{DM}, z_j) F_{\Delta\lambda, i} \Delta z_j \quad (34)$$

where  $[F_{\Delta\lambda, i}]_T$  is the flux in the chosen pass-band of the generic galaxy  $i$  of mass  $M_{G, i} = M_{BM, i} + M_{DM, i}$ , and  $\Delta z_j$  is the generic redshift range centered on  $z_j$  and defined by  $0.5 \times [z_j - z_{j-1}]$  and  $0.5 \times [z_{j+1} - z_j]$ . The number of galaxies  $N_i(M_{DM, i}, z_j)$  at the generic redshift  $z_j$  is calculated using the mass scale of the DM halos, whereas the photometric properties are obtained using the mass scale of BM and more precisely the mass in stars existing in the galaxy at the time  $t$  or redshift  $z$ . The indices  $i$  and  $j$  runs over the whole grids of masses and redshifts under considerations. The total U magnitude is shown by the dotted blue line in Fig. 8. The magnitude scale along the y-axis is on the left hand side of the figure.

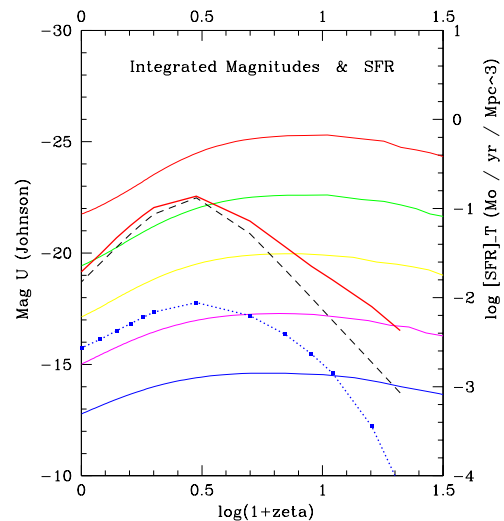


**Figure 8.** Three groups of data are displayed: (i) the integrated absolute U magnitude of the model galaxies as a function of the redshift (on logarithmic scale); each galaxy is indicated by a solid line with different color code according to the mass of the BM component. The galaxies on display have BM masses of  $10^8$  to  $10^{12} M_\odot$  from the bottom to the top of the Figure (blue, magenta, yellow, green, red). (ii) The total magnitude in the U-pass-bands of all the galaxies present in the ideal sample of  $1 \text{ Mpc}^3$  volume according to the Lukić et al. (2007) statistics (the blue dotted line with filled circles). The y-axis for the magnitudes is at left hand side of the panel. (iii) The SFRD(z) for the same sample of galaxies (the red solid line). Finally the analytical fit of the Madau & Dickinson (2014) SFRD (the black dashed line). The y-axis for the SFRD is at right hand side of the figure.

(iii) Similar procedure is applied to derive the total true SFR for the galaxies in the same ideal sample contained in a volume of  $1 \text{ Mpc}^3$ .

$$[SFRD(z_j)]_T = \sum_i N_i(M_{DM}, z_j) SFR_i(z_j) \Delta z_j \quad (35)$$

where the indices  $i$  and  $j$  run over the whole mass and redshifts grids as before. The SFRD(z) is the red solid curve. The scale for the SFR is along the y-axis at the right hand side of the figure. The SFRD(z) has the same trend of the total U-magnitude, thus confirming that the UV light is a good tracer of star formation.

The results are shown in Fig. 9 and compared with the data and the empirical best-fit relation of Madau & Dickinson (2014) given by eqn. (1) (the dotted black line).

Theory and data nearly agree in the location of the peak (redshift  $z \simeq 2$ ) and at the low redshift side (descending branch), whereas they may differ up to a factor of three beyond the peak towards the past.

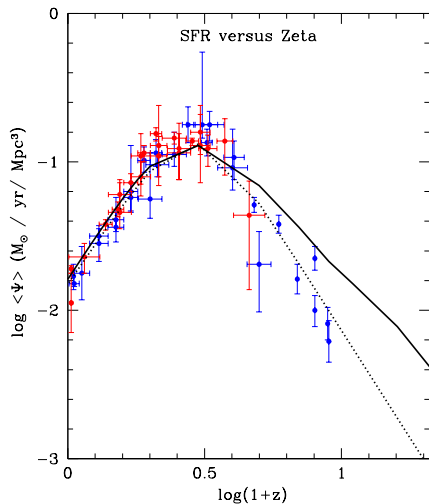


**Figure 9.** The theoretical SFRD( $z$ ) predicted from galaxy models of group B (solid black line) compared with the observational data (blue and red filled circles with error bars) and the analytical fit of Madau & Dickinson (2014) (dotted line).

The provisional conclusion we could derive at this stage is that the theoretical SFRD( $z$ ) and the data of Madau & Dickinson (2014) fairly agree each other, thus indicating that our simple model of the cosmic SFR well reproduces the observational data.

It is worth emphasizing here that for each bin of redshift, the SFRD( $z$ ) is obtained by summing up the contribution from galaxies of different mass, and in particular different history and stage of star formation. For instance in the redshift interval  $1 < z < 3$  we may have both galaxies with increasing SFR and galaxies with descending SFR. The change in the slope of the SFRD( $z$ ) at  $z \simeq 2$  implies a change in the slope of the mean SFR in the galaxy population. At  $z > 2$  galaxies with increasing SFR dominate, the opposite at  $z < 2$ , they balance each other at  $z \simeq 2$ . The SFRD( $z$ ) does not tell the behavior of individual galaxies, but only the current mean behavior of whole galaxy population (see also the discussion in Section 7.3 below).

It is also interesting to see the contribution to the SFRD by galaxies of different mass at different redshifts. This is displayed in Fig. 10, where we show the product  $SFR(z, M_G) \times N(z, M_G)$  as a function of the total galaxy mass  $M_G$  and redshift. Each line is at constant redshifts. The color code bins the lines in three groups of redshift (namely, the red lines are for redshifts  $z=20, 15, 10, 8$  and  $6$ , the green lines for  $z=4, 2, 1, 0.8$  and  $0.6$ , the orange lines for  $z=0.4$  and  $0.2$ , finally the blue dashed line is for  $z=0$ ). At high redshifts, the dominant contribution is from the low-mass galaxies, it shifts to that from higher mass galaxies at intermediate redshifts,

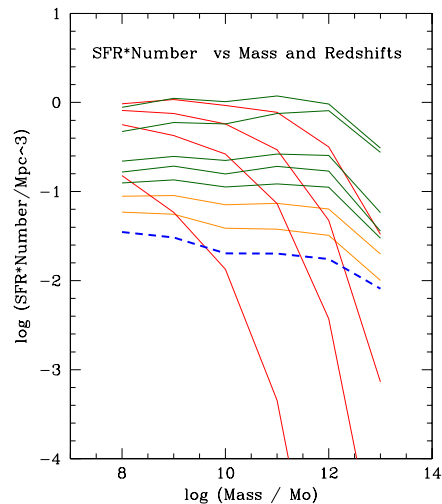


**Figure 10.** Contribution to the SFRD( $z$ ) from galaxies of different mass at varying redshifts. The red lines are for redshifts  $z=20, 15, 10, 8$  and  $6$ , the green lines for  $z=4, 2, 1, 0.8$  and  $0.6$ , the orange lines for  $z=0.4$  and  $0.2$ , finally the blue dashed line is for  $z=0$ .

and gradually it goes back to the low-mass range for redshifts tending to zero. Looking at the case  $z=0$  in the  $[SFR(M_G) \times N(M_G)]$  vs  $M_G$  plane (Fig. 10), the slope  $d \log[SFR(M_G) \times N(M_G)] / d \log M_G \simeq -0.3$  for  $M_G$  passing from  $10^8$  to  $10^{12} M_\odot$ , i.e. it mildly decreases with the galaxy mass.

To strengthen the above conclusion we look at the correlations of the SFR and SFRD( $z$ ) with the star mass  $M_s$  and/or  $M_{BM}$  as a function of the redshift. Thanks to the high efficiency of star formation ( $\nu$ ) in all the models,  $M_s \simeq 0.97 M_{BM}$ . The relationships in question are shown in the two panel of Fig. 11. The top panel shows the SFR vs  $M_s$  at different redshifts, whereas the bottom panel displays the SFRD( $z$ ) at  $z=0$ . The slope and zero point of the SFR vs  $M_s$  relationships change with the redshift. The slope gets smaller at decreasing redshift: specifically at  $z=15$  indicated by the blue line,  $z=1.0$  and  $z=0.6$  (the green and orange lines respectively) and the  $z=0$  (the dark red line). These theoretical relationships are compared by the observational one by Renzini & Peng (2015), the red solid line labelled RP15. The theoretical relation at  $z=0$  has the same slope of the one by Renzini & Peng (2015) and differs in the zero point. It coincides with the RP15 lowered by a factor of 10 (red dotted line). Model galaxies at  $z=0$  have a minimal value of star formation, therefore they belong either to the group so-called “green valley” galaxies or even to that of quiescent objects. They could rise to the values of Renzini & Peng (2015) by allowing the formation redshifts to span a wider range of values. The key result of this panel is that the slope of the SFR



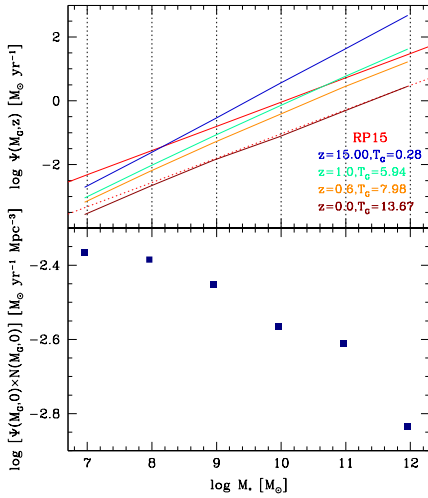


**Figure 11.** Top Panel: The SFR vs the galaxy stellar mass  $M_s$  at different epochs in galaxies of different BM mass. Since these models are without galactic winds,  $M_s \simeq 0.97 \times M_{BM}$ . The blue solid line is for  $z=15$ , the green line for  $z=1.0$ , orange line for  $z=0.6$ , and finally the dark red line for  $z=0$ . The solid red line labeled RP15 are the observational data from [Renzini & Peng \(2015\)](#) for active galaxies. Finally the red dotted line is the RP15 decreased by factor of 10 (see text for details). Bottom Panel: the product  $SFR(0) \times N(M_G, 0)$  vs mass in stars  $M_s$  of each galaxy in comoving  $Mpc^3$ .

vs  $M_s$  relation is the same as that of the observational data over a wide range of redshifts ( $0 \leq z < 1$ ). In the bottom panel the product  $SFR \times N(M_G, 0)$  decreases at increasing star mass of the galaxies. Furthermore, there may be a qualitative agreement with the data of Fig.8 of [Speagle et al. \(2014\)](#) (their Figure 8), who find that the Main Sequence slope of the star-forming galaxies increases with the redshift, i.e. the conversion of gas in stars decreases with time for all masses, the massive ones in particular. This feature, otherwise known as “downsizing” from the observational point of view, appears after a mere application of the  $N(M_G, z)$ , thus it perfectly agrees with concordance  $\Lambda$ -CDM cosmogony. Finally, there is a point to note in the bottom panel: at a first look, the case with  $M_s = 10^{11} M_\odot$  seems to deviate from the expected trend due to its apparently higher value. To single out the cause of it is a cumbersome affair. Most likely it is due to inaccuracy in the derivation of the galaxy number densities for galaxy masses in the high mass hand of the distribution. Although it is not in plain contrast with other values of stellar mass, we plan to highlight the issue investigating other halo mass functions in literature (see [Murray et al. 2013](#), and references)

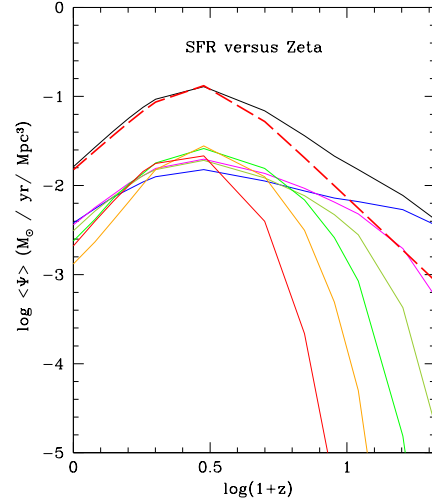


**Figure 12.** The contribution to the total SFRD(z) of Fig. 9 from galaxies of different mass. The top solid line is the theoretical SFRD(z) whereas the dashed line is the analytical fit of the data by [Madau & Dickinson \(2014\)](#). Finally the remaining lines are the partial contributions the the SFRD(z) by galaxies of different BM mass from  $10^{12} M_\odot$  (bottom) to  $10^7 M_\odot$  (top).

We conclude this section with the provisional result that our simplified model for the evolution of the SFRD(z) nicely agrees with the observational data. However, it would be of general interest to single out the physical ingredients that are ultimately responsible of this result. This will be the subject of a few ad hoc designed experiments that are shortly illustrated in the following sections.

### 7.3. Dissecting the SFRD(z)

The first test to perform is to dissect the total  $SFRD(z)$  in its components, i.e to single out the functions  $SFRD(z)_{M_G}$  whose sum at each  $z$  yields back the total  $SFRD(z)$ . These are shown in Fig.12. Remarkably, all functions peak at  $z \simeq 2$ . The decrease of the partial SFRDs at both sides of the peaks cannot be attributed only to number density (see the curves in the [Lukić et al. \(2007\)](#) and our Fig. 2) because either they are still increasing toward their peak value (case of the high mass galaxies) or they have already reached their peak at higher redshifts ( $z \simeq 5$ ) as in the case of the low mass galaxies (this mirrors the combined effects of the gravitational collapse and their destruction in the hierarchical aggregation). The only plausible explanation is that the SFRD(z) peak mirrors the superposition of the  $SFR[t(z)]$ s in existing galaxies which reach their peak in their star forming activity roughly at the same time. In more detail, back in the past ( $z > 5 - 6$ ) the dominant contribution came from low-mass objects; around

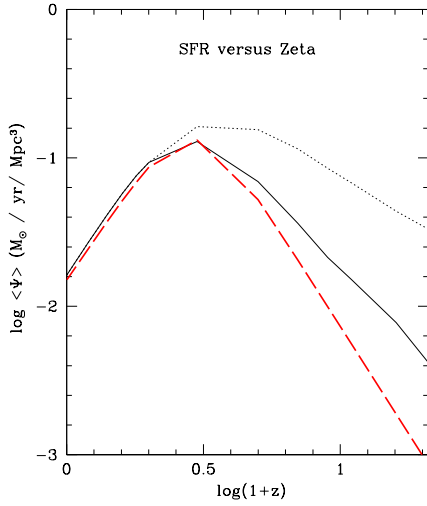


**Figure 13.** Changing the relation  $M_{BM} = \beta^{-1}M_{DM}$ . The black dotted line is the SFRD( $z$ ) derived from the arbitrary assumption that  $\beta = 1$ , equal amounts of DM and BM per galaxy. The red dashed line is the analytical best fit of the observational data of Madau & Dickinson (2014) and the solid black line the theoretical SFRD( $z$ ) of Fig. 9, obviously obtained with  $\beta = 6$ .

the peak interval all galaxies contribute in nearly equal amounts even though those with masses in the range  $10^{10}$  to  $10^{11} M_{\odot}$  are more important; finally the low-mass ones are again dominating the contribution at low redshifts ( $z < 1 - 2$ ).

#### 7.4. Changing the ratio $M_{DM}$ to $M_{BM}$

It is worth examining the effect of adopting a different ratio  $\beta = M_{DM}/M_{BM}$ . Among the various possibilities, there is one particularly interesting, i.e.  $\beta = 1$ : DM and BM are in equal amounts. The effect of this assumption on the first and second building blocks (the number of DM halos of given mass as function of the redshift, and the galaxy chemical models) are easy to foresee. The  $N(M_{DM}, z)$  distribution remains the same and no particular remark has to be made. The chemical models describing the evolution of the BM component within the DM halos remain unchanged at least with our simplified picture in which the dynamical interaction of DM and BM is neglected. Some effect would occur on the onset of galactic winds (if present) because the gravitational potential of the gas depends on the ratios  $M_{BM}/M_{DM}$  and  $R_{BM}/R_{DM}$ ; the effect is however small, not exceeding a factor of a few percent. The major difference caused by the new the relationship between BM and DM shows up when calculating  $[SFRD(z)]_T = \sum_i N(M_{DM}, z) SFR_i(M_{DM}, z) \Delta z$  because the  $SFR_i(M_{DM}, z)$  that was the SFR of the BM galaxy with mass  $M_{BM} = M_{DM}/\beta$  now is the one of

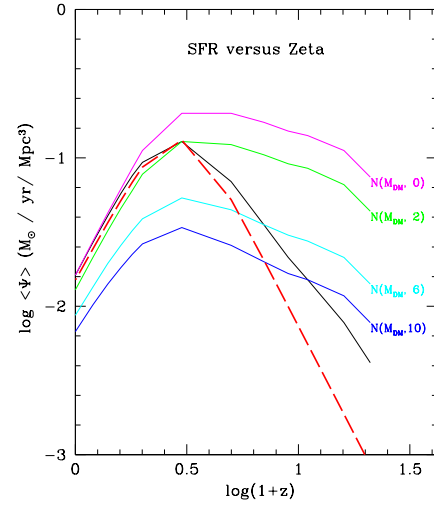


**Figure 14.** Changing the  $N(M_{DM}, z)$  relationship. See the text for details.

the BM galaxy with  $M_{BM} = M_{DM}$ : there can be a large factor in between that depends on the redshift. In other words, at given total mass  $M_G$  there is more BM to consider, so the SFR is more intense at early epochs. The new cosmic SFRD( $z$ ) and the comparison of it with the reference one and the observational SFRD( $z$ ) of Madau & Dickinson (2014) is shown in Fig. 13. The new SFRD( $z$ ) much resembles one of the reference case, nearly coincides with it on the tail from  $z=1$  to  $z=0$ , but after that it flattens out and runs well above the reference case (it peaks at about  $z=3$  instead of  $z=1$  to  $z=2$  and runs above it by a factor of about three at higher redshifts). One is tempted to argue that the cosmic SFRD( $z$ ) could be a good tracer of the amount of DM with respect to BM.

#### 7.5. Changing the $N(M_{DM}, z)$ relationship

At each redshift the gravitational aggregation of lumps of DM and BM in objects of larger and larger total mass is described by the function  $N(M_{DM+BM}, z)$  whose mass dependence is customarily approximated to  $N(M_{DM}, z)$  thanks to the large ratio  $M_{DM}/M_{BM}$ . However the exact shape of the function  $N(M_{DM}, z)$  is still uncertain, even if the one we have adopted may be a good approximation of the real one. Basing on these considerations, it comes naturally to pose the question: how would the cosmic SFRD( $z$ ) change if the underlying mass function of DM halos was different from the one currently in use? To answer the question without venturing in arbitrary speculations, we perform a simple numerical experiment. We assume that the mass distribution does not vary with the redshift but only with mass, and test four mass distributions: namely  $N(M_{DM}, 0)$ ,  $N(M_{DM}, 2)$ ,  $N(M_{DM}, 6)$  and  $N(M_{DM}, 10)$ . Therefore, while the rate of star formation in the model galaxies

**Table 4.** Characteristic quantities of the models of Group B at the onset of the galactic wind. The following quantities are shown: the baryonic mass  $M_{BM}$  in solar units, the accretion timescale  $\tau$  in Gyr, the efficiency of star formation  $\nu$ , the time  $t_{GW}$  in Gyr of the occurrence of the stellar wind, the gas fraction  $G_{g,GW}$ , star mass fraction  $G_{s,GW}$ , the current metallicity  $Z_{GW}$ , the mean metallicity  $\langle Z_{GW} \rangle$ , the SFR  $SFR_{GW}$ , the gas gravitational potential energy  $\Omega_{g,GW}$ , and the gas thermal energy  $E_{th,GW}$  at the onset of the galactic wind (both are per unit mass of the galaxy and in  $erg\ g^{-1}$ ). The top models refer to the case of standard rate of star formation and condition for galactic wind. The bottom models refer to case in which the thermal budget given to the interstellar medium is artificially cooled down to suitable value and at the same time the SFR is lowered by means of  $\nu_{eff}$  so that the galactic wind can occur only at the present time. See the text for details.

| Standard Galactic Winds and SFR |        |       |          |            |            |          |                          |            |                   |             |
|---------------------------------|--------|-------|----------|------------|------------|----------|--------------------------|------------|-------------------|-------------|
| $M_{BM}$                        | $\tau$ | $\nu$ | $t_{GW}$ | $G_{g,GW}$ | $G_{s,GW}$ | $Z_{GW}$ | $\langle Z_{GW} \rangle$ | $SFR_{GW}$ | $-\Omega_{g,GW}-$ | $E_{th,GW}$ |
| $1.0 \times 10^7$               | 6      | 10    | 0.007    | 0.010      | 0.001      | 0.0001   | 0.0001                   | 1.05E-03   | 1.72E-02          | 9.13E+00    |
| $1.0 \times 10^8$               | 5      | 10    | 0.007    | 0.011      | 0.001      | 0.0001   | 0.0001                   | 1.06E-02   | 1.75E+00          | 9.27E+01    |
| $1.0 \times 10^9$               | 4      | 10    | 0.010    | 0.011      | 0.001      | 0.0001   | 0.0001                   | 1.09E-01   | 1.80E+02          | 9.15E+02    |
| $1.0 \times 10^{10}$            | 3      | 10    | 0.010    | 0.012      | 0.001      | 0.0008   | 0.0008                   | 1.21E+00   | 2.01E+04          | 2.13E+04    |
| $1.0 \times 10^{11}$            | 2      | 10    | 0.100    | 0.030      | 0.019      | 0.0135   | 0.0083                   | 2.95E+01   | 5.22E+06          | 5.24E+06    |
| $1.0 \times 10^{12}$            | 2      | 10    | 1.010    | 0.040      | 0.362      | 0.0385   | 0.0311                   | 4.03E+02   | 5.17E+08          | 5.32E+08    |

| Modified SFR and Conditions for the onset of Galactic Winds |        |       |             |            |            |          |                          |            |                 |             |
|---|--------|-------|-------------|------------|------------|----------|--------------------------|------------|-----------------|-------------|
| $M_{BM}$  | $\tau$ | $\nu$ | $\eta_{th}$ | $G_{g,GW}$ | $G_{s,GW}$ | $Z_{GW}$ | $\langle Z_{GW} \rangle$ | $SFR_{GW}$ | $\Omega_{g,GW}$ | $E_{th,GW}$ |
| $1.0 \times 10^7$   | 6      | 10    | 0.00001     | 0.033      | 0.920      | 0.0440   | 0.0357                   | 2.89E-04   | 1.87E-01        | 1.58E-01    |
| $1.0 \times 10^8$   | 5      | 10    | 0.00010     | 0.020      | 0.928      | 0.0445   | 0.0365                   | 2.14E-03   | 1.12E+01        | 9.07E+00    |
| $1.0 \times 10^9$   | 4      | 10    | 0.00500     | 0.040      | 0.903      | 0.0488   | 0.0348                   | 1.58E-02   | 2.24E+03        | 2.07E+03    |
| $1.0 \times 10^{10}$  | 3      | 10    | 0.01000     | 0.007      | 0.928      | 0.0485   | 0.0371                   | 6.14E-02   | 3.99E+04        | 3.39E+04    |
| $1.0 \times 10^{11}$  | 2      | 10    | 0.10000     | 0.007      | 0.923      | 0.0514   | 0.0370                   | 3.42E-01   | 2.79E+06        | 2.54E+06    |
| $1.0 \times 10^{12}$  | 2      | 10    | 0.30000     | 0.008      | 0.913      | 0.0556   | 0.0366                   | 1.51E+00   | 9.24E+07        | 8.45E+07    |

varies with the redshift, their number does not. With this recipe, we calculate the corresponding SFRD(z). We will refer to this as the *false SFRDs*. The results are shown in Fig. 14. No renormalization has been applied to the false SFRD(z) to make their peak value to coincide with the observational one by Madau & Dickinson (2014). It is interesting to note that the false SFRDs resemble the real one at low redshift ( $z \leq 2$ ), strongly deviate from it at intermediate redshifts, and eventually tend again to it at high redshifts. Since the SFRs of the model galaxies are the same as those of the reference frame, this clearly shows that  $N(M_{DM}, z)$  is the term that mainly drives the shape of the cosmic SFRD(z). The gravitational building up of galaxies at early epochs ( $z \geq 1 - 2$ ) yields the rising branch whereas in more recent epochs ( $z \leq 1 - 2$ ) the declining of the mean SFR in galaxies by gas consumption most likely prevails.

#### 7.6. Changing the efficiency of star formation $\nu$

The rate of star formation we have adopted contains also the efficiency parameter  $\nu$  whose effects are worth being investigated. Figure 15 shows the SFRD(z) expected for models of type C in which the efficiency pa-

rameter  $\nu$  of the SFR is decreased from  $\nu = 10$  (top long dashed line) to  $\nu = 1$  (middle long dashed line) and even to  $\nu = 0.1$  (bottom long dashed line). Together with the observational data (filled circles) we plot the analytical fit (dotted line) by Madau & Dickinson (2014), and finally the theoretical SFRD(z) for models B (the solid black line). It is soon evident that models with a SFR too low ( $\nu = 0.1$ ) can be ruled out because too far off compared to the observational data. The agreement between theory and observational data is good for case B ( $\nu = 10$ ) and also case C models with high efficiency of SFR  $\nu = 1$  and  $\nu = 10$ , both cases, however, being somewhat higher than observed on the descending branch towards  $z=0$ .

#### 7.7. Changing the SFH of galaxies

It has repeatedly been said that an important requisite to get the observed SFRD(z) is that the star formation in galaxies starts very small, increases to a peak value and then declines because of gas consumption. How legitimate is the kind of temporal dependence of the SFR we have been using so far? In other words can we obtain the same SFRD(z) using different types of SFR?

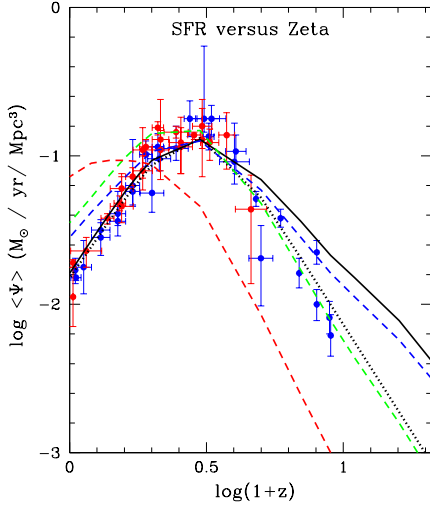


**Figure 15.** The effect of the intrinsic efficiency  $\nu$  on the SFRD( $z$ ) derived from models of the groups C (dashed lines) and B (solid line) and the comparison with observational data (filled circles with error bars) and their analytical fit (dotted line) of Madau & Dickinson (2014). The three lines for the models of group C refer to the different  $\nu$  under consideration (0.1, 1 and 10 from the bottom to the top of the figure).

To test this point, we explore here two different alternatives: (i) in each galaxy the rate of star formation is constant and equal to a suitable value so that the desired amount of stars is obtained; (ii) the rate of star formation is a mere exponentially decreasing function from a maximum value at the beginning to the present-day value.

**Constant Star formation.** The analysis is made by means of models B for which we calculate the mean SFR as

$$\langle SFR \rangle = \frac{\int_0^{T_G} \Psi(t) dt}{T_G} \Rightarrow M_s(T_G) = \langle SFR \rangle \times T_G \quad (36)$$

where  $T_G$  is the galaxy age,  $\Psi(t)$  the current SFR, and  $M_s(T_G)$  the total mass in stars at the galaxy age  $T_G$ . All these quantities are known from the previous calculation of models B. Since no galactic winds are considered in models of group B and nearly all BM mass is converted into stars ( $\simeq 90\%$ ), for all practical purposes their  $\langle SFR \rangle$  can be estimated inserting in eq.(36)  $M_s(T_G) = 0.9 \times M_{BM}$ ,  $T_G \simeq 13.5$  Gyr, and expressing it in  $M_\odot \text{ yr}^{-1}$ . With the aid of these  $\langle SFR \rangle$ , we derive the new SFRD( $z$ ) with the usual procedure and compare it with the observational one. The result is shown in Fig.16. As expected, now the cosmic SFRD( $z$ ) simply increases with decreasing redshift, thus mirroring the underlying increasing mean number density of galax-

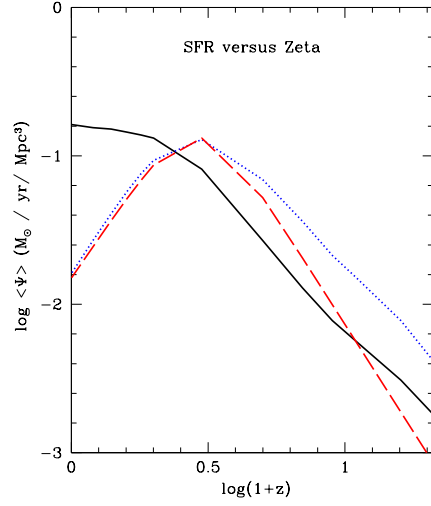


**Figure 16.** The cosmic SFRD( $z$ ) predicted by galaxy models whose rate of star formation is constant with time and equal to the mean value expected for models of group B (black solid line). The mean SFR is different for each galaxy. The value is calculated as  $M_s(T_G) = T_G^{-1} \int \psi(t) dt = \langle \Psi(t) \rangle T_G$ , where  $M_s(T_G)$  is the present day mass in stars of the galaxy with the same total mass but normal-time-varying  $\Psi(t)$ ,  $T_G$  the present day age of the galaxy. The blue dotted line is the SFRD( $z$ ) for models of group B and the red dashed line is the observational fit by Madau & Dickinson (2014).

ies of different mass. This finding lends strong support to our previous conclusion about the time dependence of the SFR taking place in each galaxy.

**Exponentially decreasing star formation rate.** To cast light on this issue we make use of the models of group A. In all these models the timescale of mass accretion and intrinsic star formation efficiency are  $\tau = 0.01$  Gyr and  $\nu = 10$ . These models closely mimic the closed-box approximation. With these assumptions, the SSFR of these models is essentially a simple exponential law. Consequently, the maximum star formation occurs at the beginning of the SFH and declines ever since. The resulting SFRD( $z$ ) is shown in Fig. 17, which shows the partial contribution to the SFRD( $z$ ) from galaxies of different mass (thin lines), the total SFRD( $z$ ), heavy solid line, and the observational fit. Looking at the total SFRD( $z$ ) we note that it is very high (actually much higher than the observational one) at high redshift, it has a lull at intermediate values and it remains lower than the observational one at low redshifts. The reason for this awkward behavior can be accounted for by examining the partial contribution from galaxies with different mass. First of all, galaxies with  $M_G > 10^{10} M_\odot$  at decreasing redshift first increase, reach a peak value and then decrease again. At  $z=0$  their contribution is comparable within a factor of five. The galaxies of lower

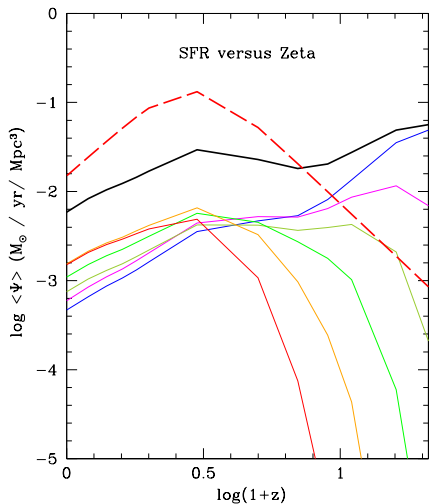


**Figure 17.** The predicted SFRD(z) for the closed-like models of type A (see text for details). The thin lines show the partial contribution to the SFRD(z) from galaxies of different mass: from top to bottom the galaxies are labelled by their BM mass scale from  $10^7$  to  $10^{12} M_{\odot}$ . The heavy solid line is the total SFRD(z). Finally, the dashed line is the analytical fit of the data by [Madau & Dickinson \(2014\)](#)

mass have, at low redshift, contribution smaller than the massive ones, the opposite happens at high redshift, and they are also responsible for the intermediate redshift lull. Finally, this can be attributed to the time dependence of the SSFR in each galaxy which is simply a mere exponential law, the same for galaxy models.

The net conclusion of this experiment is that an always decreasing SFR from an initial maximum to the present day value cannot generate the desired SFRD(z) unless other physical effects are introduced.

### 7.8. Introducing galactic winds

All the galaxy models used so far have been calculated ignoring the possible presence of galactic winds (i.e. the condition (22) for the onset of galactic winds has not been applied). In this section, we take the energy injection by supernova explosions and stellar winds into account and apply condition (22). In this view of the whole issue of galactic winds, the above prescription implies that when condition (22) is verified, the remaining gas is supposed to escape the galaxy and further star formation does no longer occur. The evolution of the remnant galaxy is a passive one and all the gas shed by stars formed in the previous epochs either in form of stellar wind or supernova explosions does no longer generate new stars. In addition to this, owing to the different gravitational potential well of massive galaxies with respect to the low-mass ones, the time at which the threshold energy for galactic winds is reached oc-

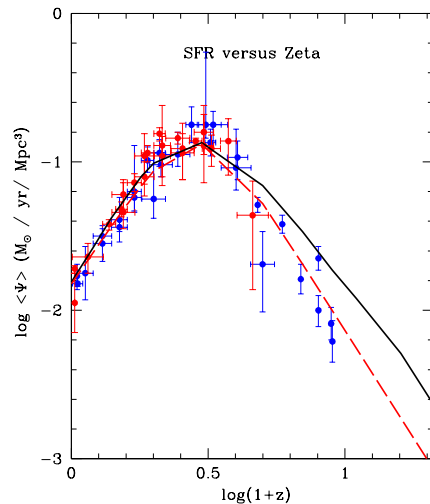


**Figure 18.** The predicted SFRD(z) for models of type B with galactic winds whose key data are reported in Table 4 and comparison with the observational data (filled circles) and their analytical fit (dashed line) by [Madau & Dickinson \(2014\)](#).

curs earlier in low-mass galaxies than in the massive ones. All this is inherent to the [Larson \(1974\)](#) model of galactic winds which has been superseded by more sophisticated treatment of the wind process with the aid of NB-TSPH models of galaxy formation and evolution ([Chiosi & Carraro 2002](#); [Merlin & Chiosi 2006, 2007](#); [Merlin et al. 2012](#)). To illustrate the point, we show in the top part of Table 4 a few key quantities for models of Group B evolved in presence of galactic winds according to the straight prescription of [Larson \(1974\)](#). With this prescription, galactic winds occur very early so that the stellar content of a galaxy is hardly made. The problem can be partly cured either by decreasing the efficiency of star formation (lower values of  $\nu$ ) or by invoking a lower quantity of energy actually injected by supernova explosions and stellar winds to the interstellar medium (more efficient cooling of this energy). Since in doing this a certain degree of arbitrariness is unavoidable owing to the lack of suitable constraints on the galaxy models in use, we prefer to adopt a different strategy.

This modeling of the galactic winds is not realistic because the numerical NB-TSPH simulations have indicated that galactic winds are not instantaneous but take place on long timescales. Gas heated up by supernova explosions and stellar winds and cooled down by radiative processes not only gradually reaches the escape velocity but also affects the efficiency of star formation because the hot gas is continuously subtracted. All this cannot be easily incorporated in the simple-minded

galaxy model we are using here. To cope with this difficulty we modify our model as follows.

First of all, feeling that the cooling algorithm we are using is not as good as the one currently adopted in NB-TSPH models, we introduce an efficiency parameter  $\eta_{th}$  ranging from 0 (no energy feed-back) to 1 (full energy feed-back) and accordingly change the (22) to the new one

$$\eta_{th} \times E_{th}(t) \geq |\Omega_g(t)| \quad (37)$$

Second we change the star formation law redefining the parameter  $\nu$  as an effective efficiency given by

$$\nu_{eff} = \nu \times \frac{|\eta_{th} \times E_{th} - |\Omega_g||}{\eta_{th} \times E_{th} + \Omega_g} \quad (38)$$

where  $\nu$  is the usual efficiency. By decreasing the efficiency of star formation at increasing  $E_{th}$  we intend to mimic the fact that hot gas is likely less prone to generate stars by gravitational collapse. As consequence, the threshold stage for the onset of galactic winds may occur much later in time or even avoided at all. Less gas is turned into stars as if part of the gas is continuously escaping from the galaxy. The net SFR decreases with obvious consequences on the SFRD(z).

New models of Group B are calculated using the efficiency parameter  $\nu_{eff}$ , and the new condition (38) for the onset of galactic winds. The values of  $\nu_{eff}$  are chosen in such a way that the galactic winds occur only at the present age or later. These parameters are listed in the bottom part of Table 4. All over their history these models have a SFR lower than their standard counterparts thus mimicking the most important effect of the energy feedback of evolving stars, i.e. heating up part of gas and subtracting it to star formation. The SFRD(z) expected from these models and the comparison with the observational one of Madau & Dickinson (2014) is shown in Fig.18. Theory and observations agree above all expectations. Although our treatment of galactic wind is very crude, yet we suspect that galactic wind should only play a marginal role on shaping the SFRD(z).

### 7.9. Changing the analytical best fit

We conclude the analysis by comparing the theoretical models with new analytical best fit of the observational data by Madau & Fragos (2017) who take into account recent data in the redshift interval ( $4 \leq z \leq 100$  and also the IMF by Kroupa (2001) instead of the Salpeter (1955) one. Changing the IMF introduces a factor 0.66 passing from the old to the new one. The comparison is shown in Fig.19. Correcting for this factor as appropriate, the agreement between theory and observation is still there.

### 7.10. Comparison with N-Body cosmological simulations

Recent attempts to model the SFRD(z) in the framework of large scale simulations of hierarchi-

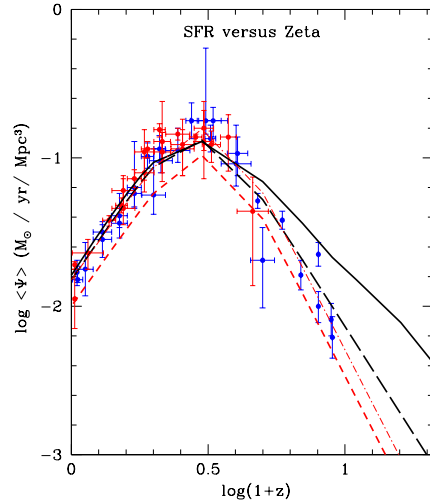


**Figure 19.** The theoretical SFRD(z) from models of group B (solid black line) compared with the observational data (blue and red filled circles with error bars), the old analytical fit by Madau & Dickinson (2014) (long dashed line), the original empirical relationship by Madau & Fragos (2017) (short dashed line) and the same shifted by the factor 0.66 to compensate for the different assumptions for the stellar IMF (dashed dotted line). See the text for details.

cal galaxy formation in  $\Lambda$ -CDM cosmogony including both DM and BM have been made possible by the new generation of numerical codes developed by Hernquist & Springel (2003b); Springel & Hernquist (2003a,b); Vogelsberger et al. (2012); Puchwein & Springel (2013); Barai et al. (2013, and references therein), in which much effort is paid to include radiative cooling and heating in presence of an UV background radiation field, star formation and associated feedback processes. The SFRD(z) in particular has been addressed by Katsianis et al. (2017, see their Fig. 7) and Pillepich et al. (2017). The key results are the comoving mean SFR and cosmic SFRD as functions of look-back time and/or redshift that are much similar to those we have used here. It is worth emphasizing that the mean SFH and SFRD(z) refer to the whole slab of Universe under examination, and not to any galaxy in particular.

In our study we have taken a different perspective: starting from galaxies of which we follow in detail the SFH, we integrate over the whole population of galaxies in the same Universe slab (which number is derived from the hierarchical growth of structures in the  $\Lambda$ -CDM cosmogony) and we derive the total SFRD(z).

In other words, starting from individual objects, we reconstruct the mean SFRD(z). In this context, the results of the present study are in perfect agreement with those obtained from extensive and time consuming cosmological simulations. The novelty of the present study

is that we arrive at the same conclusions with a much simpler approach, in which all physical foundations of the cosmic SFRD can be changed and separately analyzed with almost no computational time needed.

## 8. GENERAL REMARKS AND CONCLUSIONS

Prior to any consideration, we point out that (a) the HGF and galaxy SFR are the starring actors of the whole problem and (b) no specific assumption is made to force the galaxy models in use to reproduce the cosmic SFRD (the choice of the their leading parameter is suggested by other independent arguments). Basing on the present analysis, we may conclude:

(i) The shape of the SFRD(z) is primarily driven by the cosmic mass distribution of galaxies, i.e. the function  $N(M_G, z)$  in place at each value of the redshift. The galaxy mass distribution function in turn partly results from the growth of primordial fluctuations to the collapse stage, and partly from the aggregation of existing objects with active or quiescent star formation into new ones of larger mass (the classical hierarchical view).

(ii) The second important ingredient is the rate of star formation taking place in individual galaxies. Only the so-called time-delayed SFR, i.e. a rate of star formation that starts small, grows to a maximum and then declines, can yield the desired SFRD(z). In the formalism of the infall models, in which the BM component (in form of gas) flows into the gravitational potential well of DM at a suitable rate proportional to an exponential time dependence  $\dot{M}_{BM} \propto \exp(-t/\tau)$  and is gradually converted into stars by the law  $\dot{M}_s = \nu M_g$ , giving rise to the time-delayed star formation  $\dot{M}_s \propto \frac{t}{\tau} \exp(-t/\tau)$ . This kind of SFR is able to reproduce the one inferred in galaxies of different morphological type (see Sandage 1986; Thomas et al. 2005) and also the SFR resulting from detailed numerical NB-TSPH simulations of galaxies (Chiosi & Carraro 2002; Merlin et al. 2012). Constant and exponentially declining SFRs cannot yield the observed SFRD(z).

However, also the intrinsic efficiency of star formation (the parameter  $\nu$ ) has an important role because, together with the timescale of mass accretion, eventually drives the temporal dependence of star formation passing from the one peaking at early epochs (high values of  $\nu$ ) to that more skewed towards the present (low values of  $\nu$ ) passing through the interesting case of nearly constant star formation. We plan to better investigate this issue in a forthcoming study.

(iii) The best galaxy models to use are those of type B or even type C with minor adjustments with respect to those in use here that tend to produce too high metallicities. The problem can be easily solved either by simply changing the net metal enrichment per stellar generation (the parameter  $\zeta$  in eqn.(15)) to lower values or playing with the other model parameters  $\tau$ ,  $\nu$ , and  $\nu_{eff}$ . Since this issue is marginal to our discussion we leave it to future investigations. However, the agreement show

by type B and C models imposes a strong constraint on the type of star formation taking place in galaxies. It cannot be too much diluted over the Hubble time but instead it should be peaked at early epochs.

(iv) At early and late epochs (i.e. high and low redshifts) the major contribution to the SFRD(z) comes from galaxies of relatively low mass, whereas at intermediate redshifts the contribution from intermediate mass galaxies may parallel or even exceed that from the low-mass ones. Although always present at all epochs, the contribution from high mass galaxies is always smaller than that from low and intermediate mass ones.

(v) The energy feedback to the interstellar gas is only due to supernovae and stellar winds, no AGN has been considered. Radiative cooling of the injected energy is taken into account albeit in a simplified fashion. This point needs to be improved. The present galaxy models are not the best ones to investigate the effect of galactic winds because, owing to the one-zone approximation the onset of galactic winds at a certain time means sudden interruption of the star formation process, whereas in real galaxies and also in numerical 3D-simulations of galaxy formation and evolution, galactic winds take place locally and over very long timescales without halting star formation in the whole system. To cope with this, we preferred to decrease the efficiency of star formation as the thermal content of the gas, despite the radiative cooling, tends to approach and eventually overwhelms the gravitational potential energy of the gas. In general galactic winds, even if they improve the overall agreement of the models with observational data, are found to play a secondary role in the context of the temporal evolution of the cosmic SFRD(z).

(vi) The SFRD(z) does not represent the instantaneous SFR in individual galaxies  $\Psi_G[t(z)]$ , but it measures the mean SFR of the population of galaxies in a unit volume. Therefore, it mirrors the product  $\Psi_G[t(z)] \times N[M_G(t(z))]$ , where  $M_G$  is the total mass of a galaxy and  $t(z)$  is the particular time-redshift relation of the cosmological model of the Universe that is adopted. Using the SFRD(z) instead of  $\Psi_G[t(z)]$  to model the history of single galaxies may lead to wrong results. The opposite is also true.

(vii) We have adopted the HGF of Lukić et al. (2007), which in turn stems from the HMF of Warren et al. (2006), simply because it is an easy-to-use tool for our purposes. However, owing to the well known problem of the non-universality of the fitting function  $f(\sigma)$  (Tinker et al. 2008), other models for the HMF can be found (Murray et al. 2013). We plan to investigate this issue by using different HMFs.

(viii) The present approach yields results that fully agree with those from the highly sophisticated large scale numerical simulations. Therefore it should be considered as a complementary tool for exploring different assumptions concerning basic physical processes such as

the star formation law and the nature and efficiency of the energy feedback.

(ix) We plan to refine the present modeling of the SFRD( $z$ ) history by replacing the simple galaxy models with a library of 3D N-body simulations of galaxy formation and evolution and also the number density evolution of galaxies of different mass, i.e. the functions  $N(M_G, z)$  with the aid of ad hoc designed Monte-Carlo simulations. Finally, we will follow the photometric evolution of the galaxies to investigate the relationship between the SSFR and stellar mass content in galaxies of different mass, redshift and colors.

(x) As final conclusions we would like to shortly answer a few important questions that could be raised such as for instance: Why is the SFRD( $z$ ) small at high and low redshift? Is the quenching of SF at  $z \leq 2$  associated with a decreasing gas supply at late epochs? Why is star formation inefficient at early times even in the absence of feedback? Why is it possible to reproduce the data without AGN feedback? What is the meaning of the particular combinations of parameters  $\nu$  and  $\tau$  required to reproduce the data?

The time (redshift) dependence of the SFR in the model galaxies is the result of the cross-effect of two physical processes: the gas accretion at a suitable rate onto the galaxy potential well and the gas consumption by star formation according to a Schmidt-like law. By controlling these two parameters the galaxy models can be tuned to match the gross features of real galaxies all along the Hubble sequence. The key feature of these galaxy models is that independently of the galaxy mass the SFR starts small, grows to a maximum and then declines as function of time. However the same SFR is strong and peaked at early epochs in massive objects (having the early type galaxies as counterparts), mild and prolonged in the intermediate mass galaxies (observational counterparts the disk galaxies), and very mild and likely stretching (perhaps in recurrent bursts of activity not considered here) all over the Hubble time (observational counterparts the irregular galaxies). As already mentioned, this scheme is strongly supported by the body of observational data of galaxies and the N-body simulations of these. This tuning of the galaxy models in usage here has been made over the years independently of the cosmic SFRD issue. At low redshift, the “quenching” of star formation, is simply caused by the fact individual galaxies tend to run out of fuel (gas) in the star forming activity. At high redshift, a similar trend is recovered because galaxies are still in the gas accumulation phase and little gas has already reached

the threshold density required for star formation to occur (Krumholz 2015, it is worth recalling here that stars form in very dense environments). So at these very early epochs, the natural expectation is the star formation activity is low but growing with time. This trend would mimic the effect of some quenching at early epochs.

Our reference SFRD( $z$ ) of Fig. 9 obtained with standard energy feedback from supernovae and stellar winds, with no AGNs and no galactic winds, is already in rather good agreement with the observational one from  $z=0$  to  $z=2$  (the reference case simply mirrors the picture outlined above for the natural behavior of SFR in galaxies) whereas it tends to depart from it at increasing redshift. At redshift  $z \simeq 10$  it is about a factor of 2 to 3 higher than expected. The presence of galactic winds slightly improves the agreement in the latter region (see Fig. 18) and perhaps some other effects like mild quenching by AGNs could completely remove the discrepancy. Our provisional conclusion is that strong and exotic quenching of the star formation in the interval  $2 \leq z \leq 8$ ) (see for instance Tescari et al. 2014; Renzini 2016, and references) is not strictly needed. The only case in which either strong quenching and/or dust obscuration or both are required is when an an exponential SFR is used. However, the resulting SFRD( $z$ ) differs from the observed one in many other details and has to be discarded. Therefore, quenching does not likely play an important role in shaping the observed SFRD( $z$ ) as compared to the combined effect of the HGF  $N(M_{DM}, z)$  and of the  $\Psi(t)$  modulated by the gradual accumulation of gas within the total gravitational potential well and conversion of it into stars. It goes without saying that AGNs and galactic winds are not excluded from the above picture, but simply they are suspected to play a role less important than customarily claimed.

## ACKNOWLEDGMENTS

We would like to thank the anonymous referee for his/her useful critical comments that helped us to amend and improve the first version of the paper. C. Chiosi, F. Brotto, R. De Michele, and V. Politino are deeply grateful to the Heraeus Foundation for the financial support to attend the Heraeus Summer School 2016 “Origins of Stars and Planets” (August 2016, Florence, Italy) where this study was presented for the first time. C.C. would like to thank the Physics & Astronomy Department of the Padova University for the kind hospitality and computing support.

## REFERENCES

- Abramson L. E., Gladders M. D., Dressler A., Oemler, Jr. A., Poggianti B., Vulcani B., 2016, ApJ, 832, 7
- Alavi A. et al., 2014, ApJ, 780, 143
- Angeletti L., Giannone P., 1990, A&A, 234, 53
- Arimoto N., Yoshii Y., 1987, A&A, 173, 23
- Barai P. et al., 2013, MNRAS, 430, 3213



- Bernardi M., Shankar F., Hyde J. B., Mei S., Marulli F., Sheth R. K., 2010, *MNRAS*, 404, 2087
- Bertelli G., Bressan A., Chiosi C., Fagotto F., Nasi E., 1994, *A&AS*, 106, 275
- Bertelli G., Girardi L., Marigo P., Nasi E., 2008, *A&A*, 484, 815
- Bertelli G., Nasi E., Girardi L., Marigo P., 2009, *A&A*, 508, 355
- Bertin G., Saglia R. P., Stiavelli M., 1992, *ApJ*, 384, 423
- Bouwens R. J. et al., 2012, *ApJ*, 754, 83
- Bower R. G., Lucey J. R., Ellis R. S., 1992, *MNRAS*, 254, 601
- Bressan A., Chiosi C., Fagotto F., 1994, *ApJS*, 94, 63
- Buzzoni A., 2002, *AJ*, 123, 1188
- Cassarà L. P. et al., 2016, *A&A*, 593, A9
- Chabrier G., 2015, *IAU General Assembly*, 22, 2224239
- Chiosi C., 1980, *A&A*, 83, 206
- Chiosi C., Bressan A., Portinari L., Tantalo R., 1998, *A&A*, 339, 355
- Chiosi C., Carraro G., 2002, 335, 335
- Cucciati O. et al., 2012, *A&A*, 539, A31
- Dolag K., Jubelgas M., Springel V., Borgani S., Rasia E., 2004, *ApJ*, 606, L97
- Fattore M., 2009, PhD thesis, The University of Padova (Italy).
- Gavazzi G., Bonfanti C., Sanvito G., Boselli A., Scodreggio M., 2002, *ApJ*, 576, 135
- Gibson B. K., 1998, *ApJ*, 501, 675
- Gibson B. K., Matteucci F., 1997, *MNRAS*, 291, L8
- Gladders M. D., Oemler A., Dressler A., Poggianti B., Vulcani B., Abramson L., 2013, *ApJ*, 770, 64
- González V., Labbé I., Bouwens R. J., Illingworth G., Franx M., Kriek M., 2011, *ApJ*, 735, L34
- Gruppioni C. et al., 2013, *MNRAS*, 432, 23
- Guiderdoni B., Rocca-Volmerange B., 1987, *A&A*, 186, 1
- Guo Q. et al., 2011, *MNRAS*, 413, 101
- Hennebelle P., Chabrier G., 2011, in *Computational Star Formation*
- Hernquist L., Springel V., 2003a, *MNRAS*, 341, 1253
- Hernquist L., Springel V., 2003b, *MNRAS*, 341, 1253
- Hinshaw G. et al., 2009, *ApJS*, 180, 225
- Hopkins A. M., 2004, *ApJ*, 615, 209
- Katsianis A., Tescari E., Blanc G., Sargent M., 2017, *MNRAS*, 464, 4977
- Kodama T., Bower R. G., Bell E. F., 1999, *MNRAS*, 306, 561
- Kodama T., Bower R. G., Bell E. F., 2001, *Ap&SS*, 276, 979
- Kroupa P., 2001, *MNRAS*, 322, 231
- Kroupa P., Tout C. A., Gilmore G., 1993, *MNRAS*, 262, 545
- Krumholz M. R., 2015, *Notes on Star Formation*
- Larson R. B., 1974, *MNRAS*, 169, 229
- Larson R. B., 1991, in *Astronomical Society of the Pacific Conference Series*, Vol. 20, *Frontiers of Stellar Evolution*, Lambert D. L., ed., pp. 571–587
- Lee K.-S. et al., 2011, *ApJ*, 733, 99
- Limpert E. M., Stahel W. A., M A., 2001, *BioScience*, 51, 341
- Lukić Z., Heitmann K., Habib S., Bashinsky S., Ricker P. M., 2007, 671, 1160
- Ly C., Lee J. C., Dale D. A., Momcheva I., Salim S., Staudaher S., Moore C. A., Finn R., 2011, *ApJ*, 726, 109
- Lynden-Bell D., 1975, *Vistas in Astronomy*, 19, 299
- Madau P., Dickinson M., 2014, *ARA&A*, 52, 415
- Madau P., Ferguson H. C., Dickinson M. E., Giavalisco M., Steidel C. C., Fruchter A., 1996, *MNRAS*, 283, 1388
- Madau P., Fragos T., 2017, *ApJ*, 840, 39
- Magnelli B., Elbaz D., Chary R. R., Dickinson M., Le Borgne D., Frayer D. T., Willmer C. N. A., 2011, *A&A*, 528, A35
- Maio U., Dolag K., Ciardi B., Tornatore L., 2007, *MNRAS*, 379, 963
- Marigo P., Bressan A., Chiosi C., 1996, *A&A*, 313, 545
- Marigo P., Bressan A., Chiosi C., 1998, *A&A*, 331, 564
- Matteucci F., 1994, 288, 57
- Matteucci F., 2012, *Chemical Evolution of Galaxies*
- Matteucci F., 2016, in *Journal of Physics Conference Series*, Vol. 703, *Journal of Physics Conference Series*, p. 012004
- Matteucci F., Greggio L., 1986, *A&A*, 154, 279
- Matteucci F., Pipino A., 2002, *ApJ*, 569, L69
- Matteucci F., Tornambé A., 1987, *A&A*, 185, 51
- Merlin E., Chiosi C., 2006, *A&A*, 457, 437
- Merlin E., Chiosi C., 2007, *A&A*, 473, 733
- Merlin E., Chiosi C., Piovan L., Grassi T., Buonomo U., Barbera F. L., 2012, *MNRAS*, 427, 1530
- Mihara K., Takahara F., 1994, *PASJ*, 46, 447
- Murray S. G., Power C., Robotham A. S. G., 2013, *Astronomy and Computing*, 3, 23
- Oemler, Jr. A., Dressler A., Gladders M. G., Fritz J., Poggianti B. M., Vulcani B., Abramson L., 2013, *ApJ*, 770, 63
- Parsa S., Dunlop J. S., McLure R. J., Mortlock A., 2016, *MNRAS*, 456, 3194
- Pillepich A. et al., 2017, *ArXiv e-prints*
- Piovan L., Tantalo R., Chiosi C., 2006a, *MNRAS*, 366, 923
- Piovan L., Tantalo R., Chiosi C., 2006b, *MNRAS*, 370, 1454
- Piovan L., Tantalo R., Chiosi C., 2006c, *Mem. Soc. Astron. Italiana*, 77, 873
- Pipino A., Calura F., Matteucci F., 2013, *MNRAS*, 432, 2541
- Pipino A., Matteucci F., 2011, *A&A*, 530, A98

- Planelles S., Borgani S., Dolag K., Etti S., Fabjan D., Murante G., Tornatore L., 2013, *MNRAS*, 431, 1487
- Portinari L., 1998, PhD thesis, University of Padova, Italy, (1998)
- Portinari L., Chiosi C., 1999, *A&A*, 350, 827
- Portinari L., Chiosi C., 2000, *A&A*, 355, 929
- Portinari L., Chiosi C., Bressan A., 1998, *A&A*, 334, 505
- Press W. H., Schechter P., 1974, 187, 425
- Puchwein E., Springel V., 2013, *MNRAS*, 428, 2966
- Rasera Y., Teyssier R., 2006, *A&A*, 445, 1
- Reddy N. A., Steidel C. C., Pettini M., Adelberger K. L., Shapley A. E., Erb D. K., Dickinson M., 2008, *ApJS*, 175, 48
- Renzini A., 2006, *ARA&A*, 44, 141
- Renzini A., 2016, *MNRAS*, 460, L45
- Renzini A., Peng Y.-j., 2015, *ApJ*, 801, L29
- Saglia R. P., Bertin G., Stiavelli M., 1992, *ApJ*, 384, 433
- Saito M., 1979a, *PASJ*, 31, 181
- Saito M., 1979b, *PASJ*, 31, 193
- Salpeter E. E., 1955, *ApJ*, 121, 161
- Sandage A., 1986, *A&A*, 161, 89
- Santini P. et al., 2012, *A&A*, 538, A33
- Schenker M. A. et al., 2013, *ApJ*, 768, 196
- Schmidt M., 1959, *ApJ*, 129, 243
- Smit R., Bouwens R. J., Franx M., Illingworth G. D., Labbé I., Oesch P. A., van Dokkum P. G., 2012, *ApJ*, 756, 14
- Sobral D., Smail I., Best P. N., Geach J. E., Matsuda Y., Stott J. P., Cirasuolo M., Kurk J., 2013, *MNRAS*, 428, 1128
- Speagle J. S., Steinhardt C. L., Capak P. L., Silverman J. D., 2014, *ApJS*, 214, 15
- Springel V., 2005, *MNRAS*, 364, 1105
- Springel V., Di Matteo T., Hernquist L., 2005a, *MNRAS*, 361, 776
- Springel V., Hernquist L., 2003a, *MNRAS*, 339, 289
- Springel V., Hernquist L., 2003b, *MNRAS*, 339, 312
- Springel V. et al., 2005b, *Nature*, 435, 629
- Talbot, Jr. R. J., Arnett W. D., 1971, *ApJ*, 170, 409
- Talbot, Jr. R. J., Arnett W. D., 1973, *ApJ*, 186, 51
- Tantalo R., Chinellato S., Merlin E., Piovan L., Chiosi C., 2010, *A&A*, 518, A43
- Tantalo R., Chiosi C., Bressan A., Fagotto F., 1996, *A&A*, 311, 361
- Tantalo R., Chiosi C., Bressan A., Marigo P., Portinari L., 1998, *A&A*, 335, 823
- Terlevich A. I., Caldwell N., Bower R. G., 2001, *MNRAS*, 326, 1547
- Tescari E., Katsianis A., Wyithe J. S. B., Dolag K., Tornatore L., Barai P., Viel M., Borgani S., 2014, *MNRAS*, 438, 3490
- Thomas D., Maraston C., Bender R., Mendes de Oliveira C., 2005, *ApJ*, 621, 673
- Tinker J., Kravtsov A. V., Klypin A., Abazajian K., Warren M., Yepes G., Gottlöber S., Holz D. E., 2008, *ApJ*, 688, 709
- Tinsley B. M., 1972, *A&A*, 20, 383
- Tinsley B. M., 1980, *Fund. Cosmic Phys.*, 5, 287
- Tornatore L., Borgani S., Dolag K., Matteucci F., 2007, *MNRAS*, 382, 1050
- van der Burg R. F. J., Hildebrandt H., Erben T., 2010, *A&A*, 523, A74
- Vogelsberger M., Sijacki D., Kereš D., Springel V., Hernquist L., 2012, *MNRAS*, 425, 3024
- Warren M. S., Abazajian K., Holz D. E., Teodoro L., 2006, *ApJ*, 646, 881
- Wiersma R. P. C., Schaye J., Smith B. D., 2009a, *MNRAS*, 393, 99
- Wiersma R. P. C., Schaye J., Theuns T., Dalla Vecchia C., Tornatore L., 2009b, *MNRAS*, 399, 574
- Wilkins S. M., Trentham N., Hopkins A. M., 2008, *MNRAS*, 385, 687